AN EXPERIMENTAL AND THEORETICAL ANALYSIS OF ACTIVE VIBRATION DAMPING OF A CANTILEVER BEAM USING A DISTRIBUTED ACTUATOR

by

John M. Plump
S.B., Massachusetts Institute of Technology
(1983)

SUBMITTED TO THE DEPARTMENT OF MECHANICAL ENGINEERING IN PARTIAL FULFILLMENT OF THE REQUIREMENTS FOR THE DEGREE OF

MASTER OF SCIENCE

at the

MASSACHUSETTS INSTITUTE OF TECHNOLOGY
May 13, 1986

Signature of Author_____
Department of Mechanical Engineering
May 13, 1986

Certified by_____
James E. Hubbard Jr., Ph.D
CSDL Technical Staff, Thesis Supervisor

Accepted by_____
Ain A. Sonin
Chairman, Department Thesis Committee

AN EXPERIMENTAL AND THEORETICAL ANALYSIS OF
ACTIVE VIBRATION DAMPING OF A CANTILEVER BEAM
USING A DISTRIBUTED ACTUATOR

by

John M. Plump

Abstract

An active vibration damper which uses a distributed piezoelectric actuator, polyvinlidene flouride film, and 'bang-bang' feedback control to damp transverse vibrations in beams has been tested experimentally on a 6 inch x 0.5 inch x 0.030 inch steel cantilever beam with a 6.7 gram tip mass and a 48 inch x 6 inch x 0.1250 inch aluminum cantilever beam with a 2.04 kg tip mass. The results of tests on the first bending mode of these structures verify those results predicted by the simulation algorithm developed by Bailey. The passive loss factor of the steel beam was $\eta = 0.002$ for small amplitude tip displacements. Using the Lyapunov damper with a voltage amplitude of 100 volts increased the loss factor to $\eta_{100} = 0.046$ at a tip displacement of 0.5mm. Active damping with a 500 volt control amplitude increased the loss factor to $\eta_{500} = 0.375$ at the same displacement amplitude. The passive loss factor at small tip displacements of the aluminum beam was $\eta = 0.0019$. Lyapunov control with an amplitude of 100 volts increased the system loss factor to $\eta_{100} = 0.030$ at a tip displacement amplitude of 1.7 cm. Active damping with a control amplitude of 400 volts increased the loss factor to $\eta_{400} = 0.080$. The Lyapunov damper was also demonstrated to be very effective on the second and third bending modes of the aluminum beam. For the second mode of the aluminum beam, the initial condition was an angular acceleration at the tip of 56.5 $rad\ s^{-2}$. The Lyapunov control decreased the settling time from a free decay of 41 seconds to a controlled settling time of 7.4 seconds using a control amplitude of 400 volts. The initial condition for the third mode tests was an angular acceleration of 127 $rad\ s^{-2}$ at the tip. For the third mode the settling time was reduced from 20.5 seconds to 3.8 seconds using a control amplitude of 400 volts. These experimental results verify that the Lyapunov damping is most effective for smaller vibration levels.

A constrained layer damper which uses the PVF2 acutator as an active constraining layer was proposed as a candidate design which would be effective on damping all vibration amplitudes. The general system consisting of a base structure, viscoelastic layer and active constraining layer was modelled, resulting in a sixth order partial differential equation governing the transverse motions of the beam. The specific case of the active constrained layer damper applied to a cantilevered beam with tip mass and rotary inertia was discussed. This model revealed that the piezoelectric properties of the constraining layer contribute to the shear strain in the VEM. As a result it is possible to actively modulate the amount of energy dissipated. Also the active control appears as work at the system boundary. With the constraining layer fixed to the tip mass and left free at the root, the active portion of the stress in the constraining layer appears as a boundary moment which can do work on the system.

Thesis Supervisor: James E. Hubbard Jr.
Title: Member CSDL Technical Staff

Acknowledgements

I would like to take this time to thank Jim Hubbard for all of his support and enthusiasm during the last two years. His patience and encouragement has been greatly appreciated, and I've enjoyed working with him very much. I'd also like to thank my parents for their encouragement and David Weissburg who has been a good friend and has made my stay in Boston more enjoyable. He may someday teach me how to play saxophone.

I acknowledge the support of this thesis by the Air Force Rocket Propulsion Laboratory under contract # F04611-85-K-0050.

Contents

List of Tables

List of Figures

Nomenclature

A	Nondimensional stiffness parameter
B	Beam depth to length ratio
d_t	Tip displacement
f	Geometry parameter
g	Geometry parameter
g_2	Shear modulus of VEM
G	Dimensionless shear modulus
G_1	Storage modulus of viscoelastic material
G_2	Loss modulus of viscoelastic material
h_1	Constraining layer thickness
h_2	Viscoelastic layer thickness
h_3	Base structure thickness
J	Dimensionless rotary inertia
J_t	Rotary inertia
j	Square root of -1
L	Beam length
M	Dimensionless tip mass
M_t	Tip mass
r	Thickness to length ratio of beam with constrained layer damper
t	Time
T	Dimensionless time
u	Work done on viscoelastic layer
U	Dimensionless work done on viscoelastic layer
v	Control voltage
V	Dimensionless control voltage
V_c	Maximum control voltage amplitude
w	Beam displacement
W	Dimensionless beam displacement
x	Length measure
X	Dimensionless length measure
y	Height measure
α	Moment constant
β	Centerline separation of base structure and constraining layer in constrained layer damper
γ_2	Shear in viscoelastic layer
δ_0	Ridgid body displacement of constraining layer with respect to base structure

Δ_1 Displacement field of constraining layer
Δ_2 Displacement field within the viscoelastic layer
Δ_3 Displacement field within base structure
η System loss factor
η_2 Loss factor of viscoelastic material
θ Vibration half period
ρ Density of base structure
σ Dimensionless stress
σ_1 Tensile stress in constraining layer
σ_3 Tensile stress in base structure
τ Dimensionless shear stress
τ_2 Shear stress in viscoelastic layer
τ_3 Shear stress in base structure
ω Angular frequency

Chapter 1

Introduction

Space vehicles of the future may be quite large [1]. For many of these structures, such as telescopes or antennas, mission success may depend upon a stable platform for observation or maintaining a stable shape. Tolerances in typical optical systems can be of the order of 1/50th of a wavelength [2]. Maintaining these tolerances will require designs which are free of vibrations. As can be seen by the wealth of literature [3,4,5], vibration control in these proposed structures has received much attention. Structural vibrations in large space structures will be lightly damped due to the low internal damping of the materials used in construction, and as a consequence of their configuration. (i.e. generally a system with very little mass and stiffness which spans a large distance) Transient vibrations could be initiated as a result of attitude maneuvers, tracking, or upon spacecraft deployment and will have very long decay times. In linear systems the transient overshoot and settling time of vibrations are directly related to system damping. There may also be constant disturbances to the system due to cooling systems, reaction wheels, etc. The consequences of such vibrations are possible structural fatigue, line of sight errors in optical systems, or other system malfunctions [6].

Because of the proposed systems being very light and flexible, they can not be treated as lumped systems. These flexible structures are distributed parameter systems having an infinite number of vibrational modes. Current vibration control systems may use both active and passive elements [7]. A typical passive element is a viscoelastic dashpot. Active elements are of two types, inertial or interstructural. Examples of inertial force actuators are reaction wheels, control moment gyros or proof mass actuators.

This thesis documents ongoing research in the development of active distributed parameter vibration dampers which use a spatially distributed actuator, polyvinylidene flouride film (PVF2). A vibration damper has been designed [8] which uses PVF2 to achieve control over all transverse vibration modes of beams without truncation of the plant model. In what follows, the effectiveness

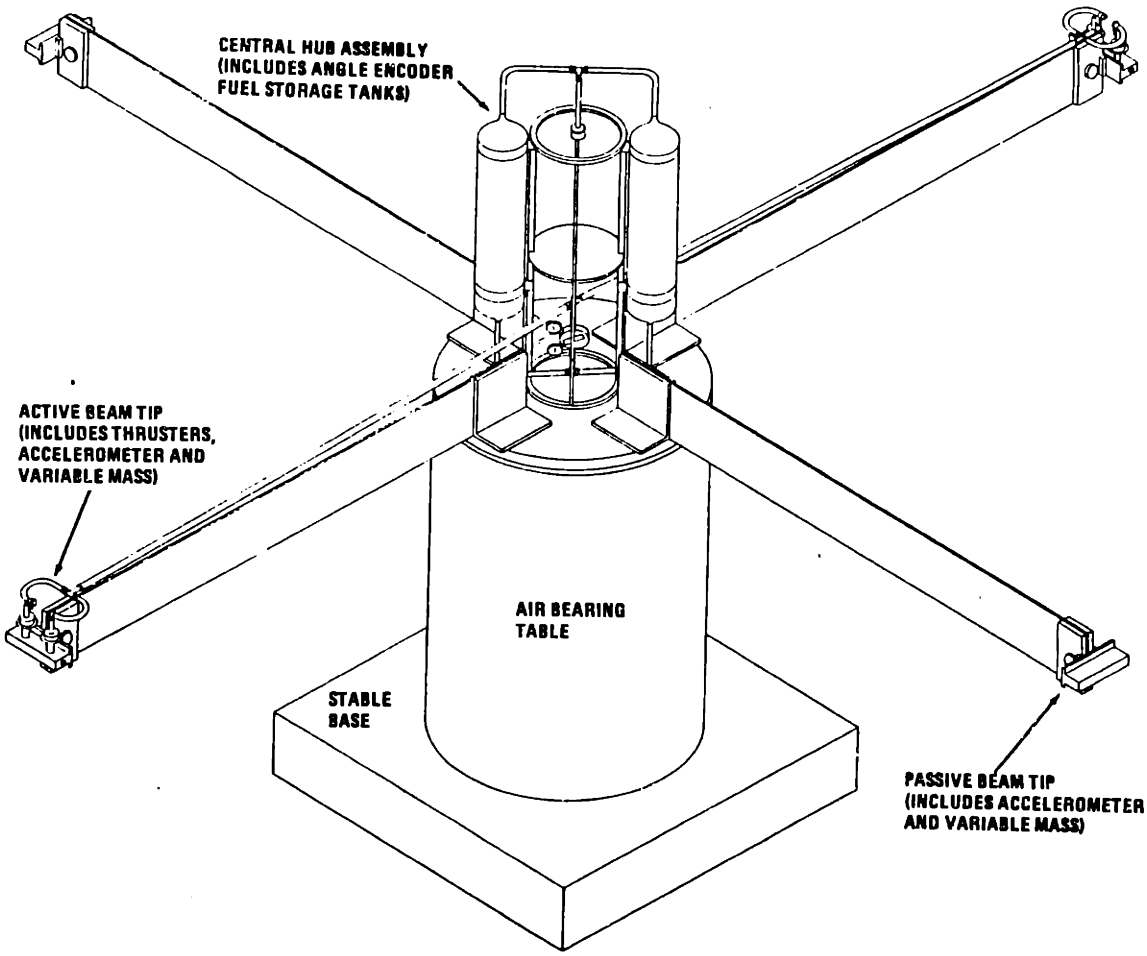

Figure 1.1: Scale Satellite Structure at the Charles Stark Draper Laboratory

of this method on a cantilever beam is experimentally verified and documented. In addition, a constrained layer damper which uses PVF2 as an active constraining layer has been developed. The modelling and proposed effectiveness of this damper are also discussed.

This work is part of an effort to damp the vibrations in a scale model satellite located at the Charles Stark Draper Laboratory [6]. This satellite structure consists of a cylindrical hub with four perpendicular appendages extending radially outward. (cf. Figure 1.1) The entire structure is mounted on an air bearing table to allow free rotation about the hub axis. Nitrogen gas thrusters are mounted on two of the arms. These are used to initiate and control slew maneuvers of the structure. The piezoelectric film dampers are being developed to damp the transverse bending oscillations of the appendages on this test structure which result from slew maneuvers.

Chapter 2

Damping of Distributed Systems

2.1 Damping of Distributed Space Structures

The inherent system loss factor in large space structures can approach the material loss factors of its components [2]. This is because many of the alternate dissipation mechanisms such as air drag, joint losses and acoustic radiation have been eliminated either by design (i.e. tight joints) or as a result of the space environment itself. Engineering analysis has addressed the problem of increasing the damping in these structures using two different approaches. They are by increasing the inherent damping of the members in the structure via some passive means, or by doing negative work on the system using active actuators.

Passive designs are appealing because of their simplicity. A passive damper dissipates energy via experiencing inelastic deformation or undergoing some other irreversible process, and is completely self contained. Passive damping can be designed into a structure by using high loss materials, or local damping elements. Use of free layer and constrained layer damping has been avoided because of the weight penalty it represents. As a result, attempts have been made to damp certain target modes by employing local shear dampers around select members or joints. This local approach, however, has been shown to yield unpredictable results, and has the other unfavorable effect of redistributing energy out of certain modes and into others [10].

There are many difficulties in using discrete actuators to control distributed structures. Since the system to be controlled is of infinite order only a finite subset of modes can be controlled using discrete actuators. The plant model is usually separated into principle modes which are to be damped, and residual modes which will not be damped [11,12]. The number of modes chosen to represent the system as well as the location of sensors and actuators is often difficult to reconcile [13,14]. Historically, active dampers used in this context have been based on the use of discrete sensors/actuators and have used colocated velocity sensor and force actuator pairs. Using this approach the amount of

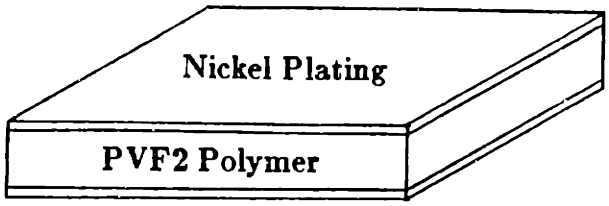

Figure 2.1: PVF2 Film with Metal Plating

damping per individual mode has been unpredictable and certain modes may experience limited damping, independent of the damping coefficient designed into the control system [7]. Another difficulty in the analysis and design of control systems for distributed systems is that the feedback loop tends to couple the initially uncoupled open loop modes. There exists the possibility of the controller exciting modes which are left out of the dynamic model. This is called control spillover and can drive the unmodeled dynamics unstable. There is also the companion effect which is called observation spillover, sensors detecting modes which have been left out of the model, causing the compensator to react to these unmodelled dyanmics. These two effects have been the subject of current research [15].

2.2 Distributed Active Damper Design using PVF2

An active vibration damper which circumvents many of the problems associated with modal truncation was developed at M.I.T. [9]. This damper uses a spatially distributed actuator and can be configured to achieve control over all bending modes in a beam [8]. Figure 2.1 shows a sketch of PVF2. The film can be caused to strain by placing an electric field across its faces. Generally a metal plating of aluminum or nickel is deposited on each face to distribute a voltage, and hence the field, along the entire surface. Spatially varying the field across the film will cause the strain to vary spatially as well. Figure 2.2 shows the configuration of the active damper developed. It is a single layer of PVF2 bonded to one side of a beam. The effect of this configuration is to produce a voltage dependent bending moment which is distributed along the beam. In this study, a cantilever beam with mass and rotary inertia at the tip will be discussed

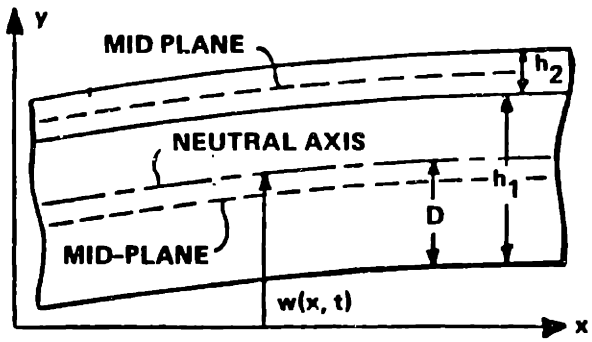

Figure 2.2: Lyapunov Damper Configuration

(cf. Figure 2.3). Also, the film and beam properties are uniform along the beam length. With the film and beam properties spatially uniform, the integrated effect of the distributed moment manifests itself as a discrete moment located at the tip of the beam.

The equations of motion for the system shown in Figure 2.3 are:

$$E_s I_s \frac{\partial^4 w}{\partial x^4} + \rho b h_s \frac{\partial^2 w}{\partial t^2} = 0 \tag{2.1}$$

with boundary conditions:

$$w = 0\big|_{x=0} \tag{2.2}$$

$$\frac{\partial w}{\partial x} = 0\Big|_{x=0} \tag{2.3}$$

$$E_s I_s \frac{\partial^2 w}{\partial x^2} = -I_t \frac{\partial^3 w}{\partial t^2 \partial x} + \alpha v(t)\Big|_{x=L} \tag{2.4}$$

$$E_s I_s \frac{\partial^3 w}{\partial x^3} = M_t \frac{\partial^2 w}{\partial t^2}\Big|_{x=L} \tag{2.5}$$

It should be noted that for this configuration the control variable only appears in one boundary condition.

A feedback control law was derived using Lyapunov's Second Method since it can easily handle bounded inputs and can be extended to distributed parameter systems [9]. The control law has been derived for a beam with no internal damping. In this study we will consider only the class of weak solutions of Equation (2.1), given boundary conditions in (2.2) and (2.3), which obey the conditions outlined by Kalmann and Bartram in [16].

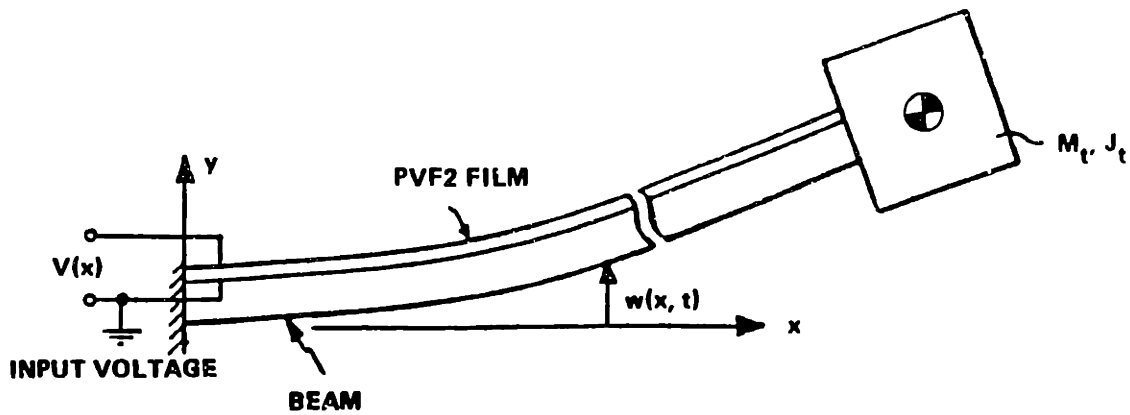

Figure 2.3: Lyapunov Damper on a Cantilevered Beam with Mass and Rotary Inertia at the Tip.

A suitable Lyapunov-functional for the above model is,

$$F = \frac{1}{2}\int_0^L \left(\frac{\partial^2 w}{\partial x^2}\right)^2 + \left(\frac{\partial w}{\partial t}\right)^2 dx \tag{2.6}$$

where the first term in (2.6) is a measure of the strain energy in the structure and the second term is a measure of its kinetic energy. With this choice of F conditions which are at least sufficient for stability can be derived. [17], [18].

A control law is found which will control all modes of vibration using only angular velocity at the tip of the beam as the feedback variable. The resulting control algorithm is given as;

$$v(t) = -Sgn\left(\frac{\partial^2 w}{\partial t \partial x}\bigg|_{x=L}\right) \cdot V_c \tag{2.7}$$

where V_c is the bounded control voltage. For a decaying periodic input, this controller commands a constant amplitude square wave, or "bang-bang" control output.

An obvious disadvantage of this law is that it is non-linear and hence may lead to sliding mode problems and/or limit cycles depending on how well the physical system approximates the assumptions necessary for Lyapunov stability as mentioned earlier. A digital simulation and parametric study was performed which implemented the Lyapunov control law.

2.3 Simulation of the Lyapunov Control Law for a Single Mode

The simulation algorithm is as follows:

1. Start with the beam having some initial displacement amplitude in a single mode, and an initial velocity of zero.

2. For each half-cycle of vibration, determine the amount of work done on the beam by the active damper and the energy dissipated by any passive damping in the system.

3. Subtract the amount of energy lost during the half cycle from the amount of energy in the system at the beginning of the half cycle. Use the remaining energy to determine the corresponding displacement amplitude of the beam.

4. Repeat steps 2 and 3 until the displacement amplitude reaches zero.

This algorithm assumes that the control will not significantly change the mode of vibration, and while it does not include the effects of air damping it does augment the model by adding passive damping in the form of a passive loss factor η which accounts for any internal structural damping which may be present. The first mode of vibration and the Lyapunov control law were chosen to demonstrate the simulation. The tip displacement represents the modal displacement. This simulation algorithm essentially gives the decay envelope of the vibration since the displacement amplitudes are determined every half cycle.

Chapter 3

Experimental verification of Lyapunov control

3.1 Test Structures

The Lyapunov control algorithm derived in [9] has been experimentally tested on two different structures. The first is a 6 inch x 0.5 inch x 0.030 inch steel beam, which is a dynamically scaled bench top version of one of the arms on the model satelite structure. The second test was on one of the model satelite structure arms. This was a 48 inch x 6 inch x 0.1250inch aluminum beam. Both beams were configured as cantilevers with a mass and rotary inertia at the tip. Details on the dynamic scaling of the steel beam may be found in [9]. The dimensions and physical properties of the aluminum beam and the dynamically scaled steel model are given in Table 3.1. To obtain a clear understanding of how the damper performed, it was tested on structures vibrating in a single mode. The first bending mode was chosen because it was easiest to isolate and

	Aluminum	Steel
Modulus, E, (Nm^{-2})	$76x10^9$	$210x10^9$
Length, L, (m)	1.22	0.146
Thickness, h, (mm)	3.18	0.381
Width, b, (cm)	15.2	1.27
Tip Mass, M_t, (kg),	2.04	$6.73x10^{-3}$
Tip Inertia, J_t, (kgm^2)	$1.1x10^{-2}$	$5.0x10^{-7}$
Density, ρ, (kgm^{-3})	2840	7800

Table 3.1: Beam Properties Used in Lyapunov Damper Tests

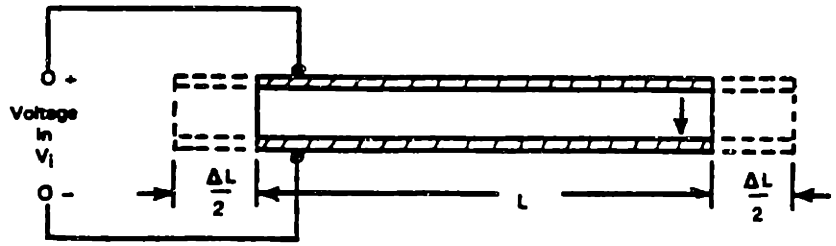

Voltage in, results in strain out

Figure 3.1: PVF2 Piezoelectric Response

Modulus, E, (Nm^{-2})	$2.0x10^{9}$
Static Piezoelectric constant, d_{31}, (mV^{-1})	$22x10^{-12}$
Thickness, h_3, (m)	$23x10^{-6}$
Density, ρ, (kgm^{-3})	1300

Table 3.2: PVF2 Film Properties

visually identify.

The tests used uniaxially polarized film, obtained from Pennwalt Corporation, King of Prussia, PA. It was bonded to both beams using a thin layer of Eccobond 45 LV epoxy. A uniaxially polarized film exhibits a longitudinal strain when an electric field is applied across its faces. [1] (cf. Figure 3.1). The physical properties of the PVF2 film appear in Table 3.2 [19]. This simple damper configuration has a uniform geometry and a spatially uniform control voltage is applied along its length. The effect of a voltage applied to the film has been shown to produce a bending moment which is distributed along the beam [20]. Because the properties of the film are uniform along the beam length, the distributed moment is spatially uniform as well.

3.2 Experimental Equipment

Figure 3.2 is a schematic layout of the equipment used in the tests of the 6 inch steel beam. The beam was fitted with a tip mass which included an

[1] A biaxially polarized film will strain along its length and width when subjected to an electric field.

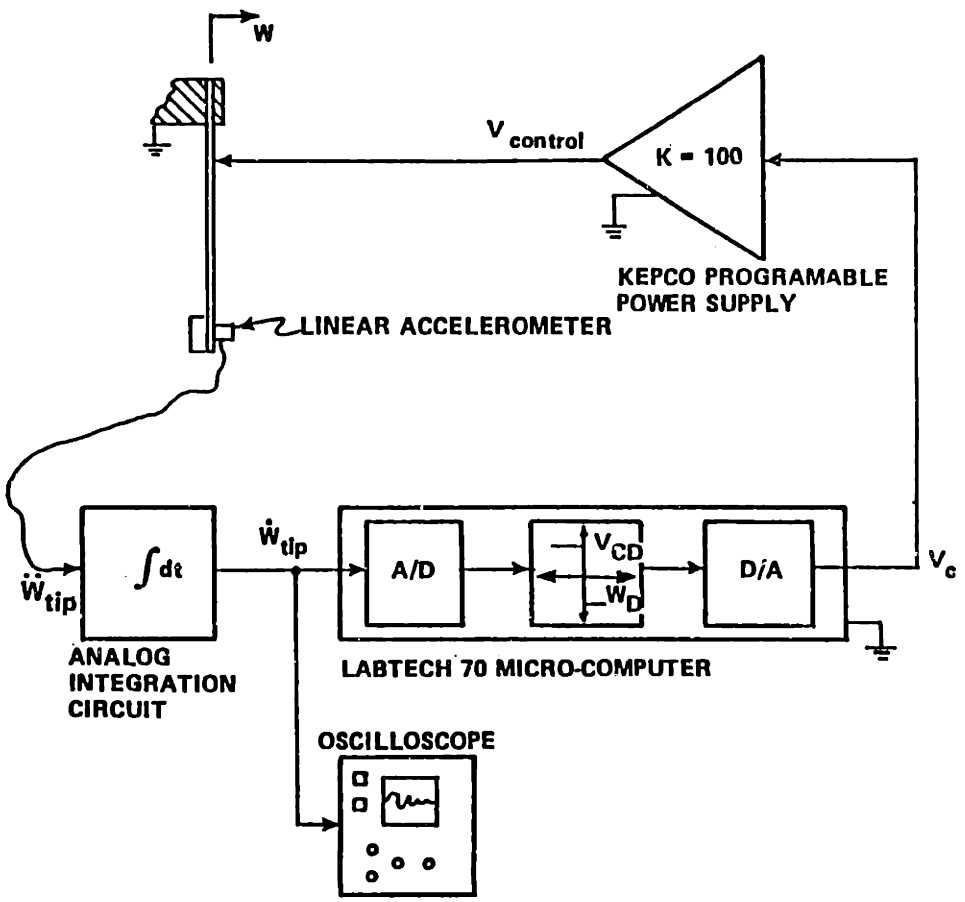

Figure 3.2: Experimental Equipment used in Steel Beam Damper Tests

Entran 0.5 gram piezoresistive linear accelerometer. The accelerometer output was integrated to give linear tip velocity, and connected to a digital oscilloscope and to the controller. The Lyapunov control algorithm was implemented via a Laboratory Technologies digital computer using a sample rate of 1000 Hz. [2] The control signal calculated by the microcomputer was amplified by a KEPCO programmable power supply. The amplifier output was applied to the PVF2 by soldering a wire to a thin, square metal washer. The washer was then clamped to the beam. To insure a good electrical contact, a silver filled, electrically conductive ink, Amicon C-931-40 was used between the PVF2 and the washer. (cf. Figure 3.3)

The passive damping of the laminated beam was determined using the logarithmic decrement method. For large tip amplitudes (on the order of 2.0cm),

[2]The first bending mode of the scaled cantilever beam was approximately 6 Hz.

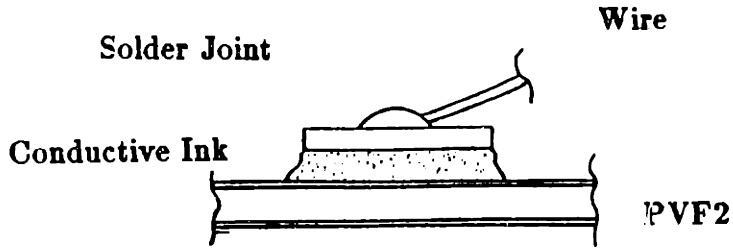

Figure 3.3: Lead Attachment Technique using Silver Filled Ink

the passive loss factor was determined to be $\eta = 0.003$. [3] For small amplitudes (1mm), the passive loss factor was less than 0.002. The larger loss factor at large tip displacements may be the result of operating beyond the linear range of the material. Application of the film to the beam did not significantly alter the passive damping in the structure, which was ignored in the derivation of the mode shapes and frequencies. The effects of passive damping were included in the simulation as an exponential decay envelope on the transient responses.

Before the damping tests were made, the distributed moment constant, α, of Equation (2.4) was determined experimentally. For these tests d.c. voltages were applied to the beam/PVF2 system, and the tip displacement measured using a fotonic sensor. Because the distributed control acts as a discrete moment at the beam tip, the effective coupling of the control to the beam could be calculated using a simple statics calculation. [21].

$$d_t = M_b \cdot \frac{L^2}{2E_3I_3} \tag{3.1}$$

$$\alpha = \frac{2d_tE_3I_3}{L^2v} \tag{3.2}$$

The observed moment constant was: $\alpha = 2.14\text{x}10^{-7}\,(Nm)V^{-1}$.

The Lyapunov control algorithm uses as input the angular velocity of the beam tip. Under single mode conditions, the linear velocity at the tip is proportional to angular velocity by a constant factor. Since only one mode of the scaled beam was assumed present, it was possible to use the linear velocity of the tip as the controlling input.

3.3 Scaled Steel Cantilever Beam Results

The tests were performed by initially displacing the tip of the beam 2 cm, releasing it, and recording the tip velocity signal with a digital oscilloscope.

[3] For linear structures, $\eta = 2 \cdot \zeta$

Dimensionless Length	$X = \frac{x}{L}$
Dimensionless Displacement	$W = \frac{w}{L}$
Dimensionless Control Voltage	$V_l = \frac{\alpha v L}{E_3 I_3}$
Dimensionless Time	$T = t \cdot \sqrt{\frac{EI}{\rho b h_3 L^4}}$

Table 3.3: Nondimensional Parameters

Although in a strict sense this type of excitation will excite all modes to some degree, only the first mode frequency was observable in the accelerometer output signal.

Figure 3.4 shows oscilloscope traces of tests for various control voltages. The figure gives a global perspective of the effectiveness of the active damper as the control voltage amplitude, V_c of Equation 2.7, was varied from 0 volts to 500 volts. As can be easily seen, the settling time is decreased from a free decay time of over 2 minutes to a damped settling time of 8 seconds.

To facilitate comparison with simulations, the beam properties were nondimensionalized using the relationships given in Table 3.3. Figure 3.5 is a plot of both simulation and experimental results showing the decay envelopes for several control voltages. A more detailed discussion of these results is defered to Section 3.6.

3.4 Aluminum Cantilever Beam Results

Tests of the active damper were also performed on the aluminum beam. Prior to laminating the film to the beam, a modal analysis was performed. This was done to identify the frequency, damping, and mode shape of the first five modes of the beam. The tests were performed using a Hewlett-Packard 5420 Structural Analyzer. The first five mode shapes appear in Figure 3.6. Table 3.4 contains the frequency and damping data of these modes.

For the active damper tests, the tip mass of the aluminum beam was fitted with an Endevco angular accelerometer and Sundstrand Q-Flex linear accelerometer. This was necessary because the angular velocity of the tip for the first mode was small. This is due to the small angular displacement at the tip (cf. Figure 3.6) and the very low frequency of the first mode. To accurately sense all modes, both the linear and angular accelerometers were used. The linear accelerometer was limited to sensing only the first mode by low pass filtering the output. The outputs were then integrated and summed to produce

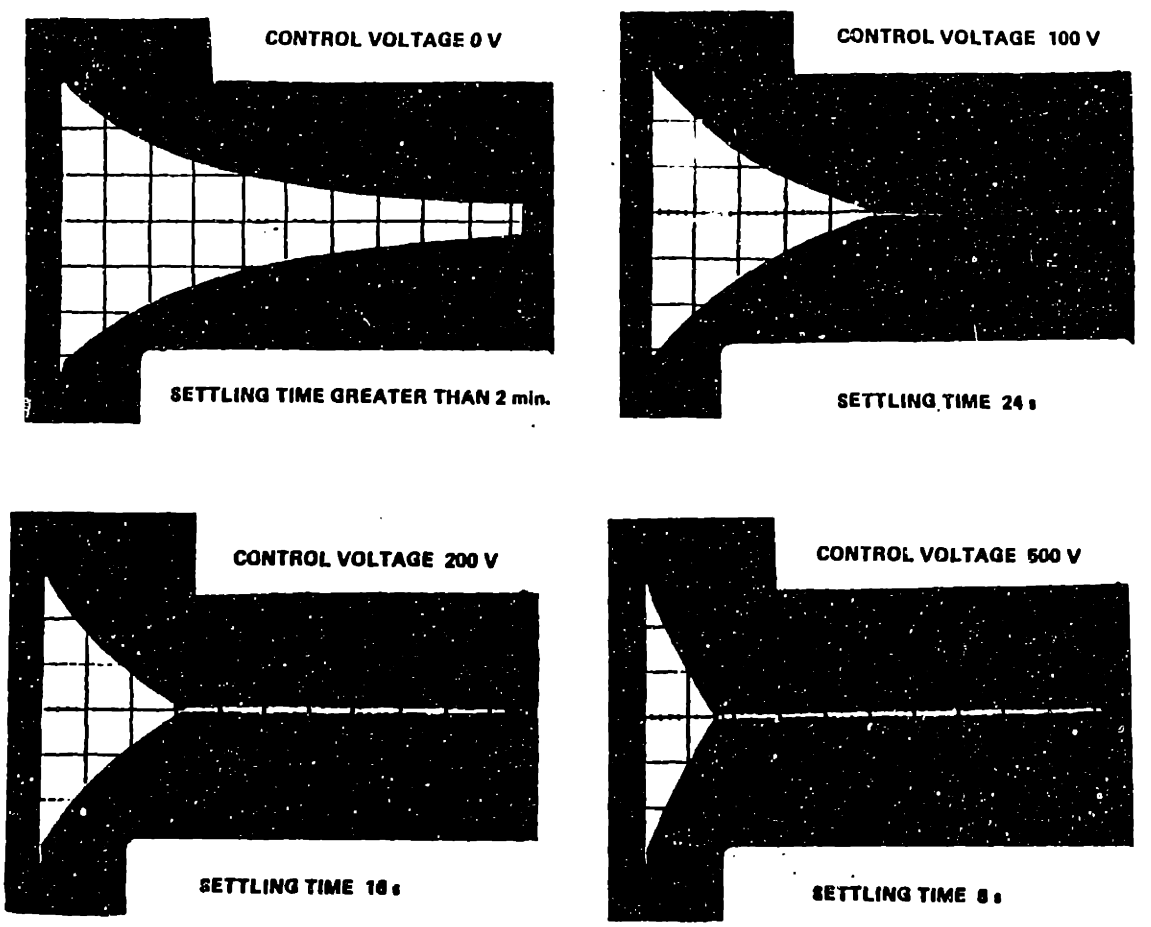

Figure 3.4: Damping Tests on First Mode of Steel Beam

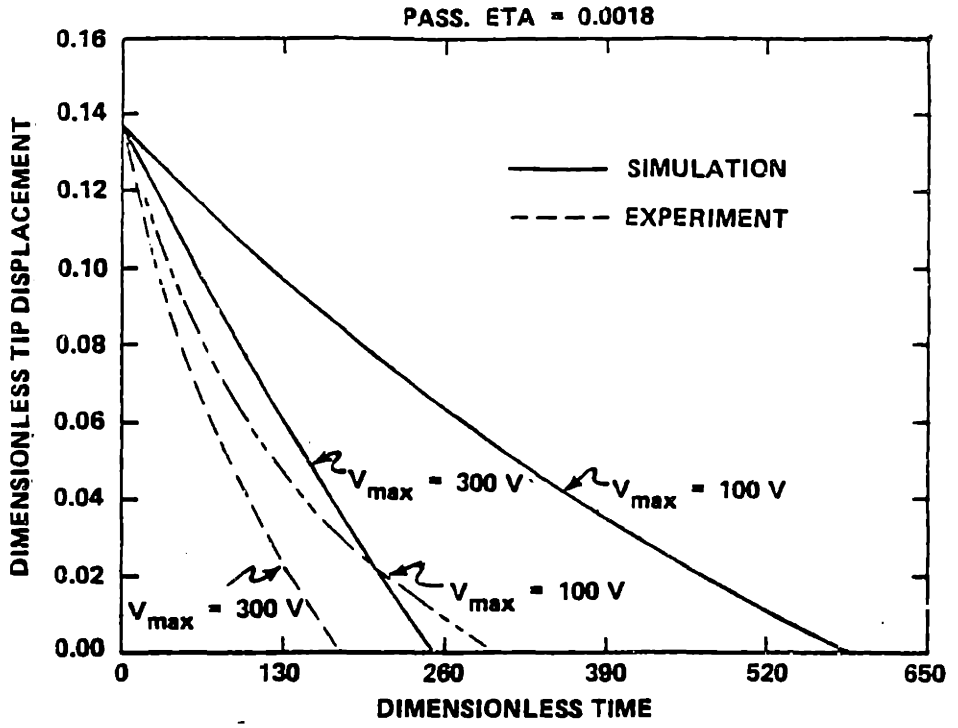

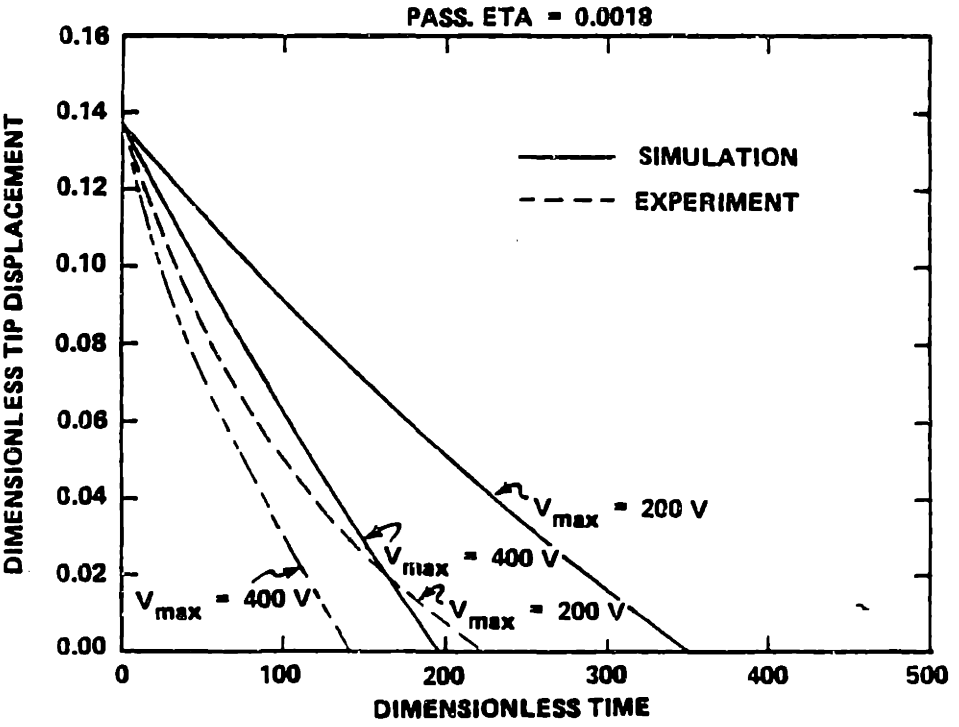

Figure 3.5: Experimental and Simulated Decay Envelopes for the 6 inch Test Structure

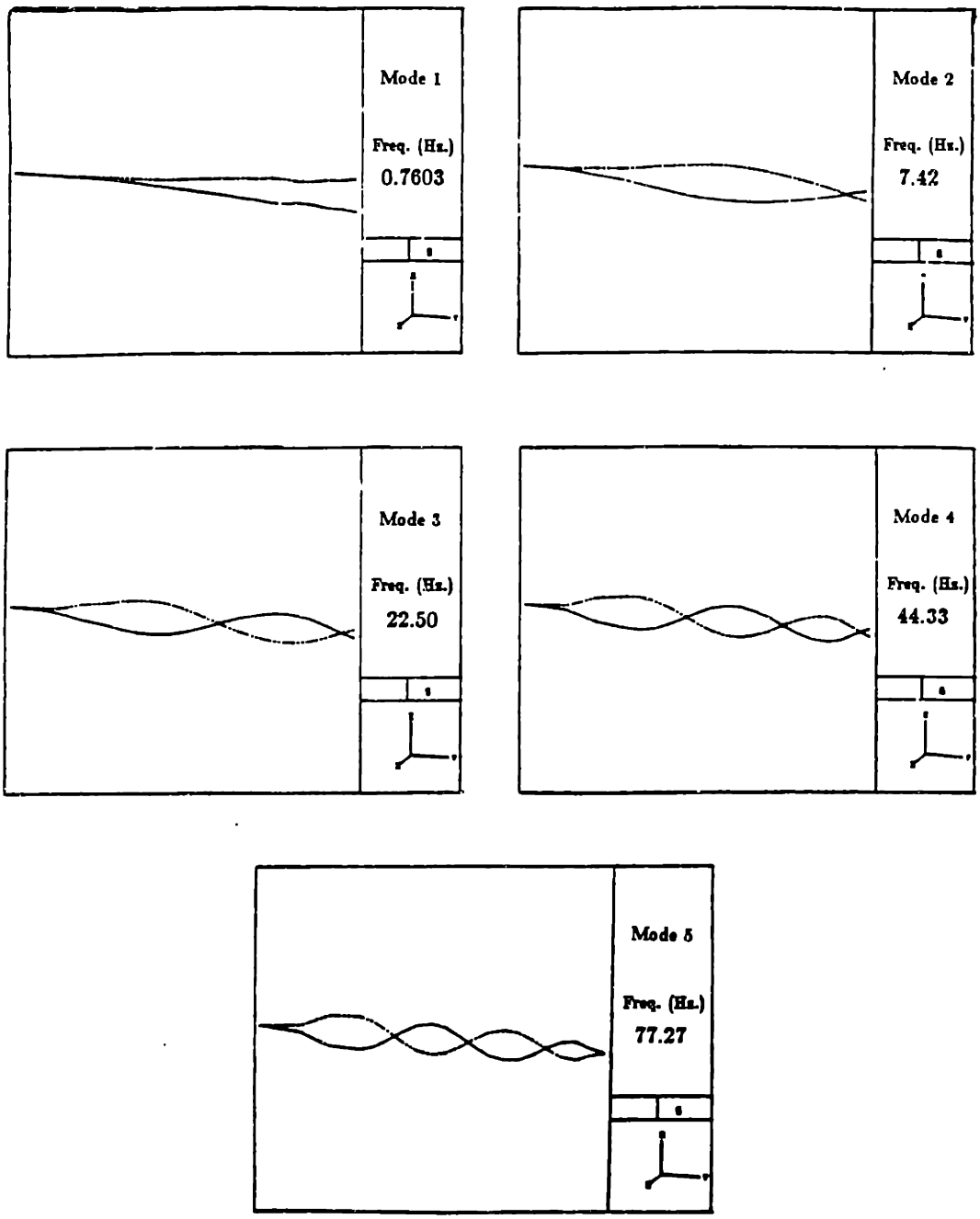

Figure 3.6: First 5 Mode Shapes of the Aluminum Test Structure

Mode Number	Frequency (Hz)	Loss Factor (η)
1	0.7603	0.0019
2	7.42	0.0048
3	22.50	0.0037
4	44.33	0.0079
5	77.27	0.0075

Table 3.4: Frequency and Damping for first 5 modes of Aluminum beam

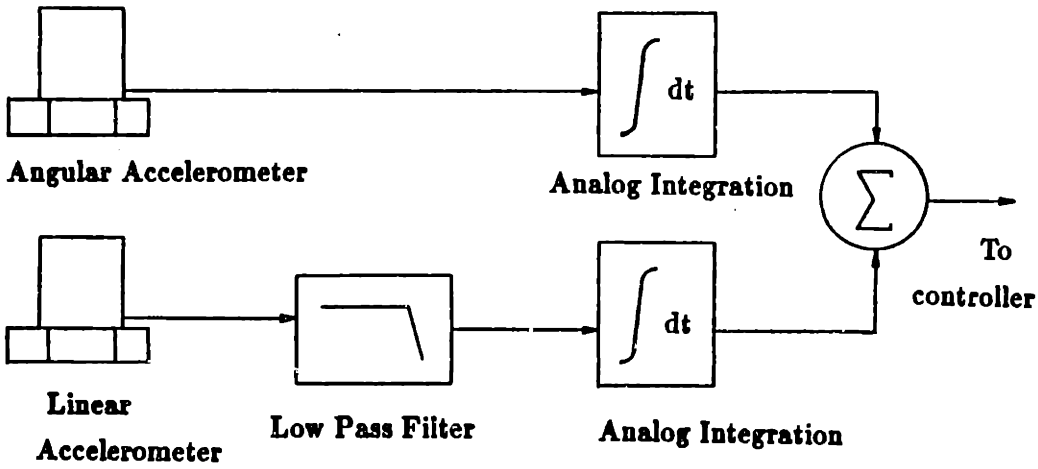

Figure 3.7: Sensor Configuration Used in Aluminum Beam Tests

the control input. Figure 3.7 shows this sensor configuration schematically.

The moment constant of the large beam was determined experimentally using the proceedure described for the 6 inch beam. The moment constant was found to be: $\alpha = 2.11\text{x}10^{-5}\,(Nm)V^{-1}$.

Preliminary tests of the active damper on the large beam showed that relatively low control voltages (220 volts) could cause electrical arcing on the film surface and localized burning of the nickel plating on the film. This burning caused the plating to become discontinuous, creating sections of the plating which were electrically isolated from adjacent sections. PVF2 will strain if it is within an electric field. Since the control voltage was applied to the system at only one location, a continuous conductor is necessary to distribute the voltage to insure a continuous distributed moment. It was determined that the arcs were being caused by current transients induced by the controller. Because the beam/PVF2 system acts like an electrical capacitor, large current transients

would be necessary for the voltage across the film to follow the Lyapunov control law. This problem was not evident with the 6 inch beam because the capacitance, and therefore the current transients, were much less. The problem was eliminated by coating the entire exposed surface of the PVF2 with the conductive ink. This was done using by applying thin coats of the ink with an air brush. Using this technique, further arcing was greatly reduced, and film with damaged plating could be repaired.

First mode tests using the aluminum beam were made by displacing the beam tip 16.7 cm and releasing it. Figure 3.8 shows time plots of tip displacements for various control voltages. Once again the effect of the control is quite pronounced with the settling time being decreased from over 409 seconds to a damped settling time of 126 seconds. To facilitate comparison with simulations, the beam properties were also nondimensionalized using the relationships given in Table 3.3. Figure 3.9 is a plot of both simulation and experimental results showing the decay envelopes for several control voltages.

3.5 Higher Mode Results

The Lyapunov controller was also sucessfully applied to the second and third bending modes of the aluminum beam. For these higher mode tests the PVF2 was used to establish the initial condition. The film was used to drive the beam by using the Lyapunov control algorithm with positive (destabilizing) feedback, rather than negative feedback. In this configuration the control would sense the modes which had been excited and drive them rather than damp them. Isolated modes were excited by giving the beam a displacement disturbance near a known anti-node of the mode of interest. The control would then preferentialy drive this mode. This is a consequence of using the Lyapunov controller. It detects and damps the mode with the largest angular velocity at the tip. With the controller acting in a positive feedback loop it continually excited the mode with the largest angular velocity. After a time, all the vibrational energy in modes not being driven was dissipated due to natural damping, and the system would be left vibrating in a single higher mode. This technique guaranteed that the system would be excited in a natural mode.

Tests were run by establishing an initial condition, and then enabling the active damping. Passive damping for the second mode was found from modal analysis to be $\eta = 0.0048$. The initial condition for all second mode tests was a peak angular acceleration at the tip of 56 $rad\, s^{-2}$. The effect of the Lyapunov damper was to reduce the settling time from over 40 seconds to 7.4 seconds using a control amplitude of 400 volts. The results of the second mode tests appear in Figure 3.10.

Passive damping in the third mode was found to be $\eta = 0.0037$. The initial condition for all third mode tests was a peak angular acceleration at the tip

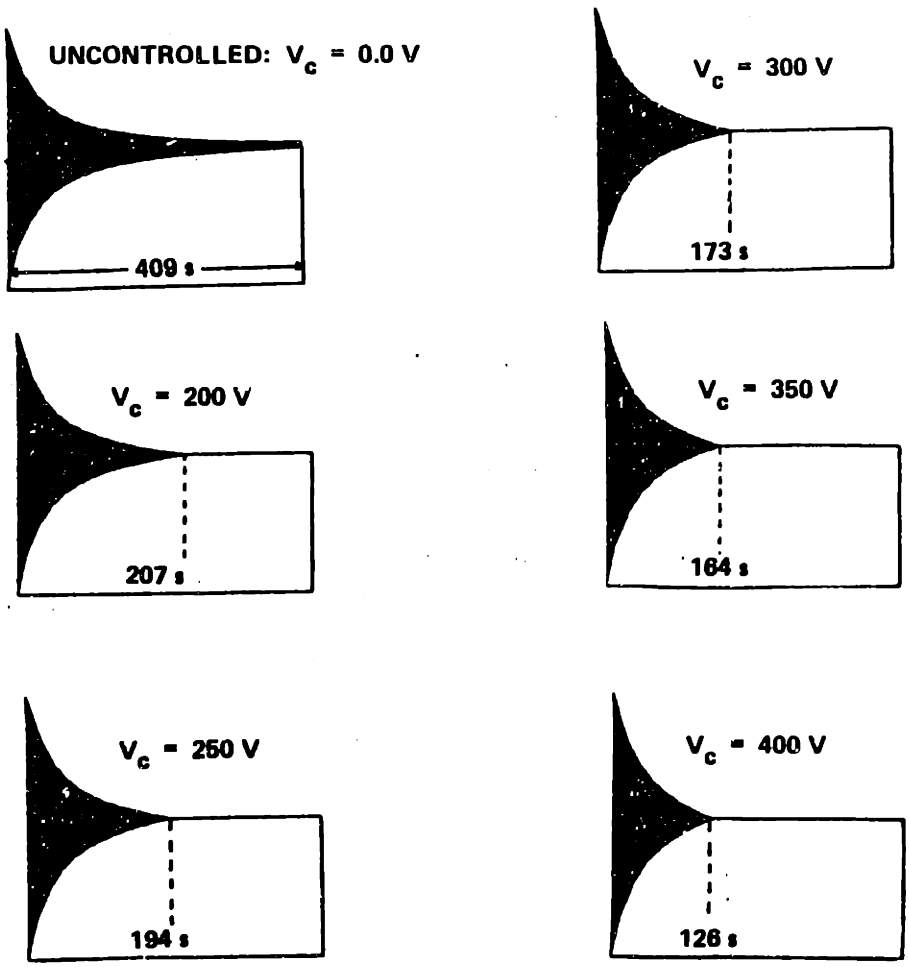

Figure 3.8: Results of Damping Tests on the First Mode of the Aluminum Structure

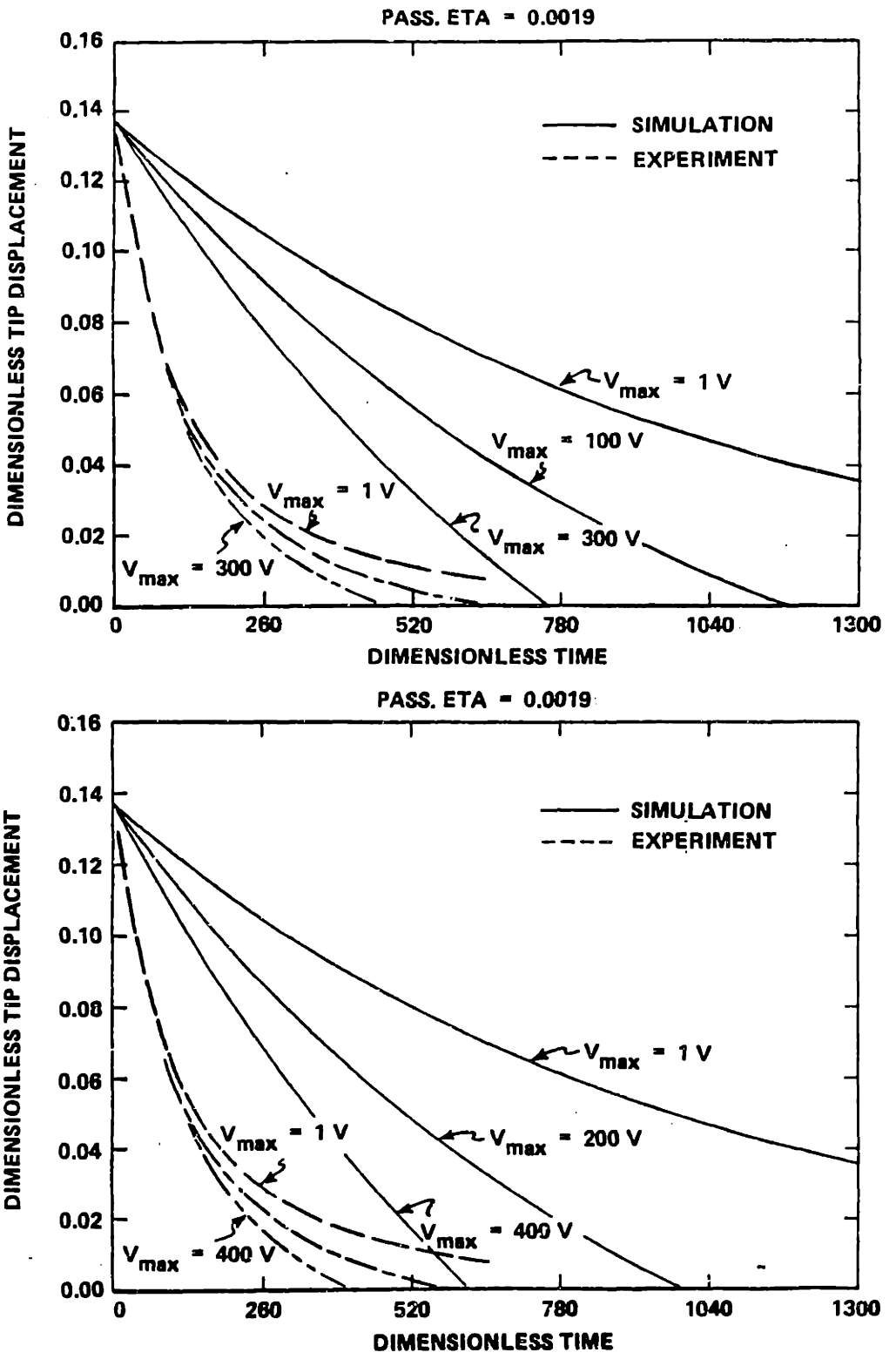

Figure 3.9: Experimental and Simulated Decay Envelopes for the Aluminum Test Structure

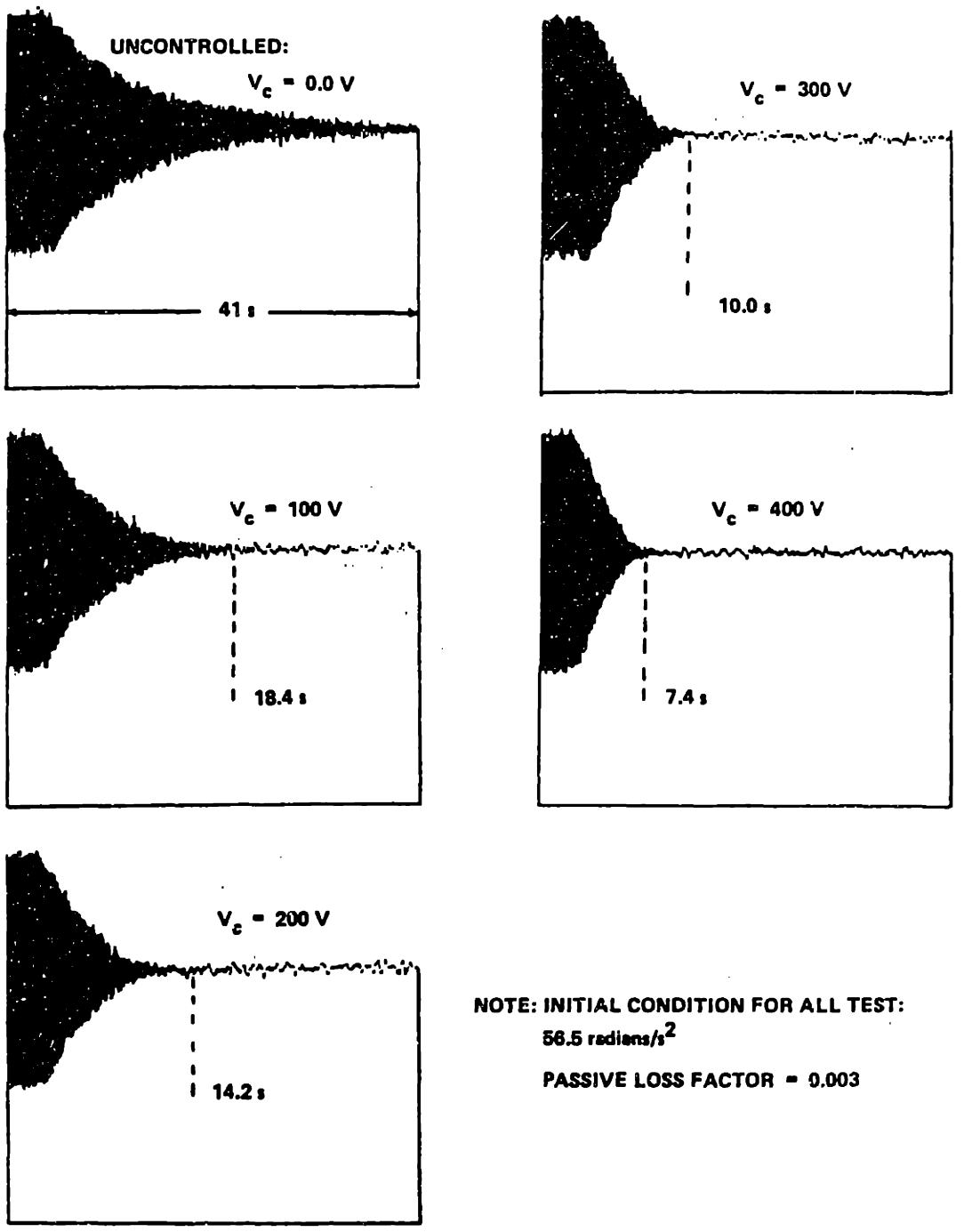

Figure 3.10: Results of Damping Tests on Second Mode of Aluminum Beam

of 127 $rad\ s^{-2}$. For this mode, active damping decreased the settling time from 20 seconds to 3.8 seconds using a control amplitude of 400 volts. The results of the third mode tests are presented in Figure 3.11. No simulation was performed for the higher modes.

3.6 Discussion of Lyapunov Control Effectiveness

The Lyapunov controller has been demonstrated to be effective on two different scale structures. The resulting damping of this nonlinear control algorithm is amplitude dependent. Consider the response of a beam with no internal damping. The application of the Lyapunov damper would cause the vibration amplitude to decay linearly in time. The resulting linear decay envelope indicates a changing effective loss factor, which increases as the vibration levels decrease. The active damping is most effective for smaller vibration levels because an actuator with a nonlinear control law such as this one dissipates an increasing percentage of the system energy as the vibration amplitude decreases. Even though the amount of energy dissipated per cycle is decreasing, the amount of energy in the system is decreasing faster.

The initial slope of all experimental decay envelopes are steeper than their corresponding predictions. This result is expected and is due to the presence of additional, unmodelled loss mechanisms being present in the physical structure. These added losses could be the result of air drag, structural nonlinearities, and/or losses occuring in the mounting fixture. As the tip amplitude decreases, however, the effects of these other damping mechanisms become negligible and the energy dissipation is primarily due to the active damping which results from the control. The final slope of the decay envelope is predicted by the simulation to be:

$$\frac{\Delta d_t}{|\Delta t|} = \frac{V_c \cdot f}{g \cdot \theta} \tag{3.3}$$

where f and g are parameters defined in [9] which are dependent on the beam geometry, material, and boundary conditions, and θ is the half period of vibration. A comparison of decay envelopes between simulation and the steel beam experiments show the final slopes to be identical, with the final settling time shifted due to the initial effects of added damping at large displacements. At lower control voltages and large amplitudes, passive damping is the dominant dissipation mechanism, while the active damping supplied by the PVF2 is dominant at small amplitudes of vibration. At the higher control voltages active damping begins to dominate the overall response of the beam. This is evident by the gradual flattening out of the decay envelopes as the displacement amplitude decreases.

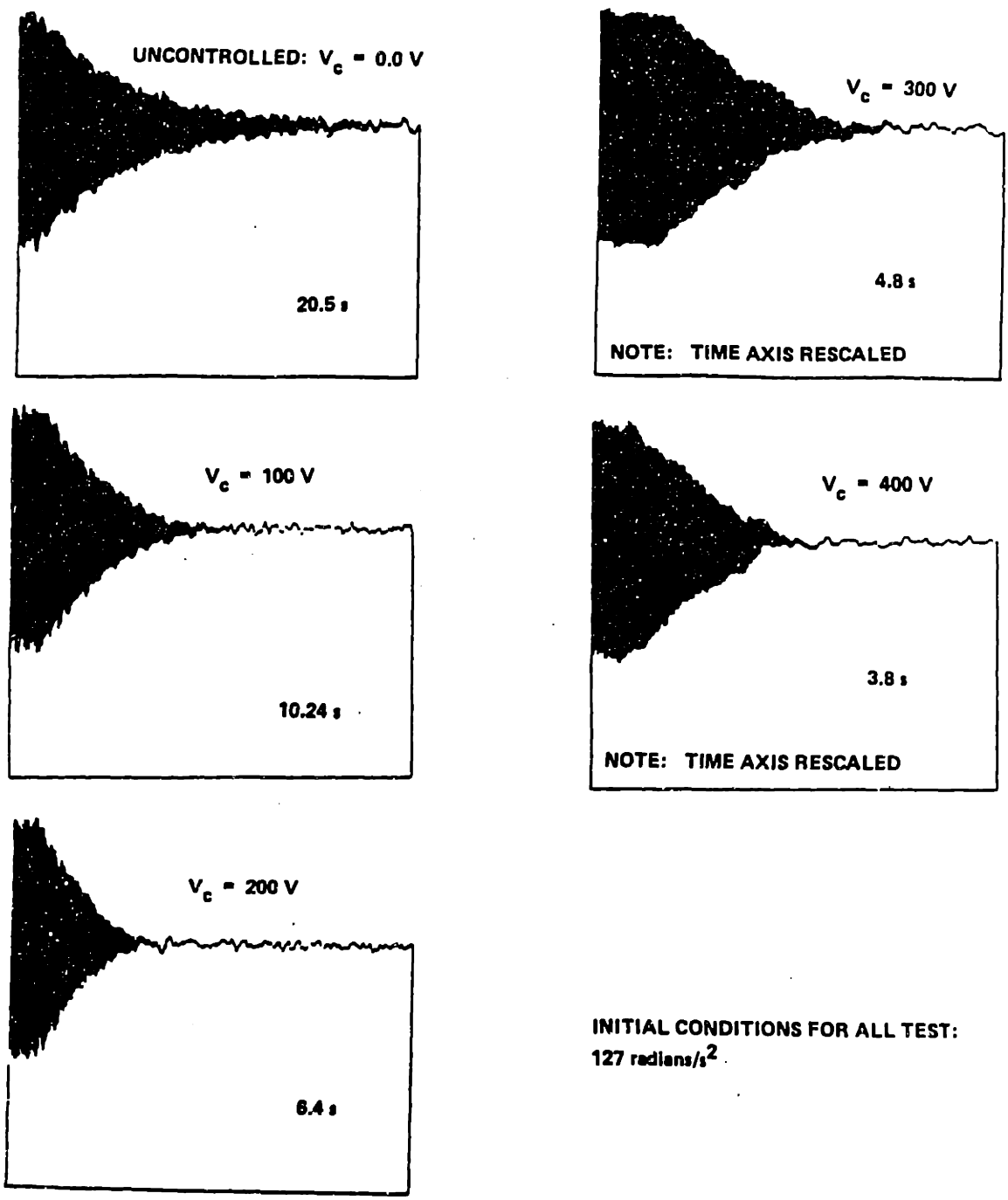

Figure 3.11: Results of Damping Tests on Third Mode of Aluminum Beam

The loss factor of the controlled structure was determined experimentally when the tip displacement amplitude was 0.5 mm. With a control voltage amplitude of 100 volts, the loss factor was $\eta_{100} = 0.046$. The loss factor when using 200 and 500 volt control amplitudes was $\eta_{200} = 0.087$, and $\eta_{500} = 0.375$ respectfully.

A comparison was also made between the predictions of the simulation and the experimental results of the full scale beam (applied to the first bending mode). Figure 3.8 is a plot of tip displacement vs. time for the full scale beam whose dimensions were given in Table 3.1. The results are almost identical to those obtained for the dynamically scaled beam. The effect of unmodelled damping, however, is much more evident, and persists over a much broader range of tip displacements. At small tip displacements where the active damping is expected to dominate, the slopes of the decay envelopes converge to the same value as expected. There is, however, a slight difference between the final slopes as predicted by Equation (3.3) and the experimental results. This difference is believed to be due to parameter uncertainties associated with aluminum beam.

The passive loss factor of the aluminum beam for small tip displacements was $\eta = 0.0019$. Lyapunov control with an amplitude of 100 volts increased the system loss factor to $\eta_{100} = 0.030$ at a tip displacement amplitude of 1.7 cm. Active damping using a control amplitude of 400 volts increased the loss factor to $\eta_{400} = 0.080$ at the same vibration amplitude.

These experimental results support the analysis and simulation done in [9] and indicate that an active damper with this type of control law may provide a method of keeping resonant vibrations from building up due to the extremely high levels of damping that can be achieved for low level vibrations. Similarly, the use of the film to excite the beam gives a clear understanding of just how this weak actuator can be used effectively. As an actuator operating in a regime which is damping controlled, this weak actuator is able to cause quite large responses.

Chapter 4

Active Constrained Layer Damper Design

4.1 Constrained Layer Dampers

Although the performance of the Lyapunov damper previously discussed has been shown to be effective at low amplitude vibration levels, a design is sought which will be effective at all levels. An active damper would need relatively powerful actuators to be effective on large amplitude vibrations. This is because of the large amount of potential energy present. PVF2 is a relatively weak actuator, and it's limited effectiveness on damping large displacements has been demonstrated. Possible damper designs which would be effective on all vibration levels could incorporate very powerful actuators for large amplitudes and the Lyapunov control for low levels, but this is at the cost of increased complexity. An alternate design philosophy is to increase the passive damping of the structure. The level of passive damping has been shown to be the primary dissipation mechanism for large amplitude vibrations. Therefore the simplest design would call for increased passive damping to control the large amplitude vibrations, which would be augmented by the active damper at low vibration levels.

The primary methods of increasing the passive damping in a distributed structure are free layer and constrained layer viscoelastic damping. Both methods rely on the strain of a viscoelastic material (VEM) to dissipate energy (cf. Figure 4.1). In a free layer damper the dilatation strain is of the same order as the shear strain [22]. If the VEM is covered with a stiff constraining layer, it experiences much greater shear and relatively small dilatation. Since most of the energy is dissipated by shear in the damping layer, using a constraining layer is very effective [23]. A simple way of incorporating the active properties of PVF2 into a constrained layer design would be to substitute a layer of PVF2 into the design as the constraining layer.

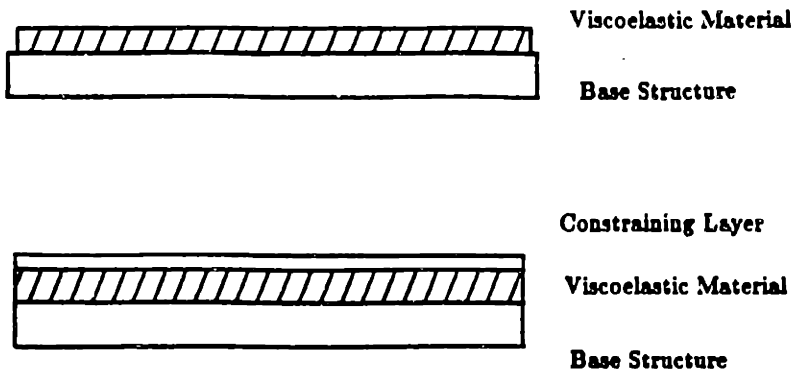

Figure 4.1: Free and Constrained layer dampers

The prospect of an active constraining layer is attractive because it allows the shear in the viscoelastic layer to be modulated actively, thereby increasing the damping effectiveness over a broader operating range. With a passive constrained layer damper, the shear, and therefore the rate of energy dissipatation from the structure, tends toward zero as the vibration amplitude decreases. Also, passive constrained layer dampers are designed for a single target mode. With an active constraining layer it would be possible to have a finite dissipation rate at low amplitudes. There also exists the possibility of combining the large amplitude performance of a constrained layer damper with the low amplitude performance of the Lyapunov controller in one design.

This chapter discusses the modelling of an active constrained layer damper which uses PVF2 as the constraining layer. It expands themes developed in [24].

4.2 Theoeretical Model Development of an Active Constrained Layer Damper

The modelling of an active constrained layer damper is presented. The result is a sixth order partial differential equation governing the transverse bending motion of a damped, finite length beam. In addition, a cantilevered beam with a mass and rotational inertia located at the tip will be discussed.

The geometry of the system being modelled is shown in Figure 4.2. Subscripts 1, 2, and 3 refer to the constraining layer, viscoelastic layer and beam layer respectively. The model is based on the following assumptions:

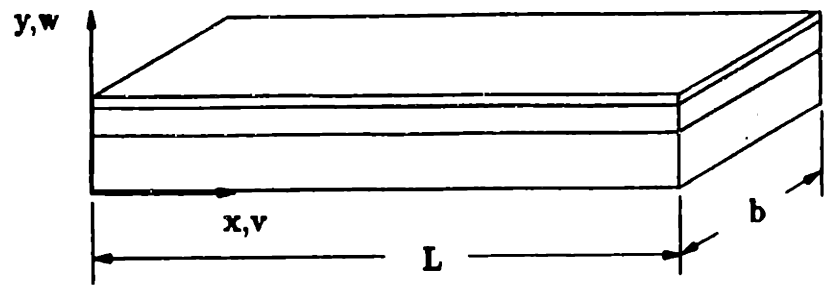

Figure 4.2: Beam Section with Constrained Layer Damper

1. The constraining and viscoelastic layers have no bending stiffness.
2. The viscoelastic layer can only transmit shear.
3. All dissipatation losses occur within the VEM.
4. There exists a uniform state of shear in the VEM.
5. Uniform normal stress throughout the thickness of the constraining layer.
6. Rotational inertia of the beam is ignored. (i.e. Bernoulli-Euler beam theory)
7. The beam and film properties are spatially uniform.

The proceedure will be:

1. Derive the strain field within the VEM.
2. Satisfy equilibrium and compatibility.
3. Introduce boundary conditions.

Consider an element of a beam in bending (cf. Figure 4.3). The displacement of a point on the surface of the beam can be decomposed into two terms. One associated with the displacement due to the slope of the beam and the second term due to the strain of the neutral axis itself. Let Δ_3 be the displacement of a point on the top surface of the element in bending. Then Δ_3 is given by Equation (4.1).

$$\Delta_3(x) = \left(\int_0^x \frac{\sigma_3}{E_3} d\eta - \frac{\partial w}{\partial x}\right) \cdot \left(\frac{h_3}{2}\right) \tag{4.1}$$

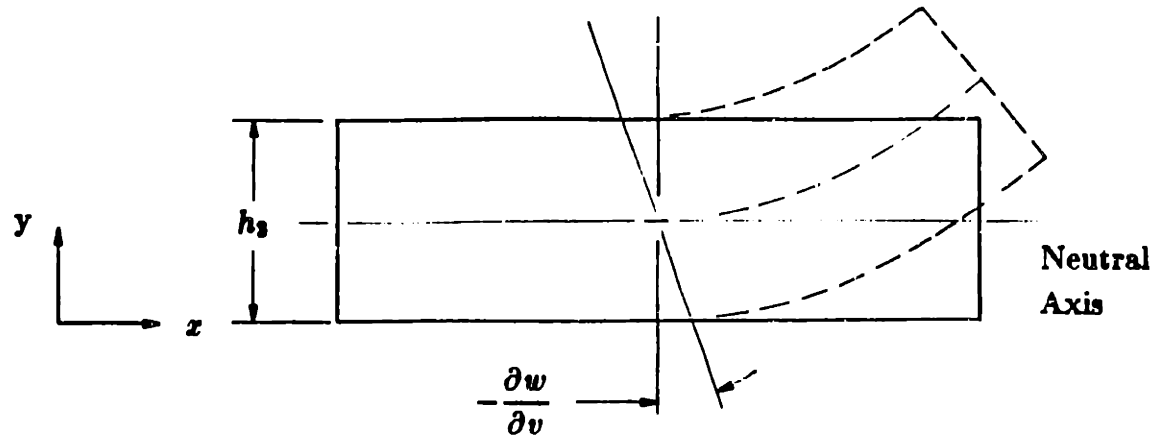

Figure 4.3: Beam Element in Bending

The displacement field of the constraining layer, Δ_1 is also composed of two terms. One is the rigid body translation of the constraining layer relative to the base structure and will be designated δ_0. A second term is due to the strain of the constraining layer. The strain in the constraining layer is caused by the mechanically induced stress, σ_1, and as a result of its piezoelectrical properties, $\frac{d_{31}}{h_1}v$. (Equation (4.2))

$$\Delta_1(x) = \delta_0 + \int_0^x \left(\frac{\sigma_1}{E_1} + \frac{d_{31}}{h_1}v\right) d\eta \tag{4.2}$$

The displacement field within the viscoelastic material, Δ_2, is the linear interpolation between layers 1 and 2, and is given by Equation (4.3).

$$\Delta_2(x) = \Delta_3(x)\left(\frac{(h_3 + h_2 - y)}{h_2}\right) + \Delta_1(x)\left(\frac{(y - h_3)}{h_2}\right) \tag{4.3}$$

The shear strain in the VEM is found by differentiating the displacement field and is given by Equation (4.4). The resulting shear stress in the VEM is given by Equation (4.5).

$$\gamma_2(x) = \frac{\partial \Delta_2(x)}{\partial y} \tag{4.4}$$

$$\tau_2(x) = g_2\gamma_2(x) \tag{4.5}$$

The free body diagram in Figure 4.4 shows the stresses on a differential element of the composite beam. The force balance equations in the x and y

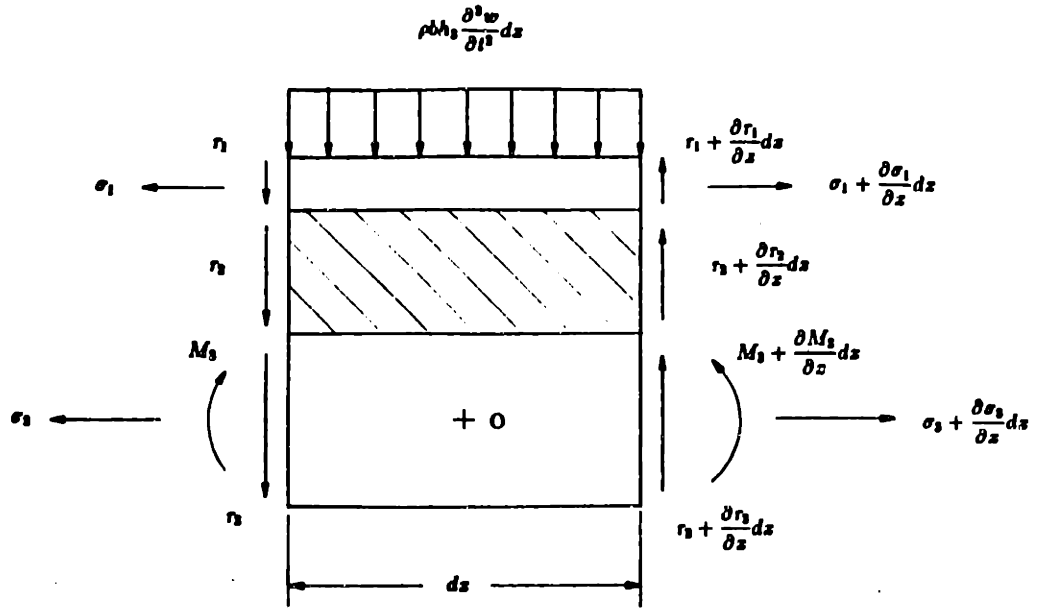

Figure 4.4: Free Body Diagram of an Element of a Damped Sandwitch Beam

directions are given by (4.6), and (4.7). Moment equilibrium of the element about point O is given by Equation (4.8).

$$h_1\frac{\partial \sigma_1}{\partial x} + h_3\frac{\partial \sigma_3}{\partial x} = 0 \tag{4.6}$$

$$-\rho h_2\frac{\partial^2 w}{\partial t^2} + h_1\frac{\partial \tau_1}{\partial x} + h_2\frac{\partial \tau_2}{\partial x} + h_3\frac{\partial \tau_3}{\partial x} = 0 \tag{4.7}$$

$$\tau_1 h_1 + \tau_2 h_2 + \tau_3 h_3 + \frac{1}{b}\frac{\partial M_3}{\partial x} - h_1\beta\frac{\partial \sigma_1}{\partial x} = 0 \tag{4.8}$$

Combining these equations and the moment-curvature relationship of a beam in bending (Equation (4.9)) yields;

$$M_3 = E_3 I_3\frac{\partial^2 w}{\partial x^2} \tag{4.9}$$

$$\frac{\partial^4 w}{\partial x^4} + \frac{\partial^2 w}{\partial t^2} = \frac{\partial^2 \sigma_1}{\partial x^2} \tag{4.10}$$

Finally, a relationship between the stress in the constraining layer and the beam deflection is needed to complete the model. Force equilibrium on the differential element of the constraining layer shown in Figure 4.4 yields Equation (4.11).

$$\tau_2 = \frac{\partial \sigma_1}{\partial x} \tag{4.11}$$

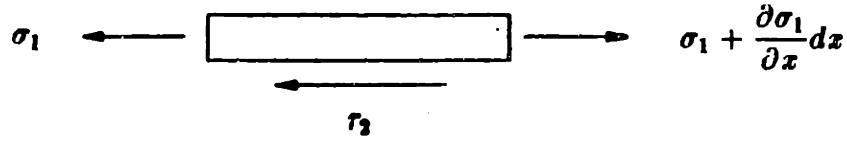

Figure 4.5: Free Body Diagram of Constraining Layer

Combining this expression with Equations (4.3), (4.4), and (4.5) and differentiating yields:

$$\frac{\partial^2 \sigma_1}{\partial x^2} = \frac{g_2}{h_1 h_2}\left[\frac{h_3}{2}\frac{\partial^2 w}{\partial x^2} + \sigma_1\left(\frac{1}{E_1} + \frac{h_1}{h_3 E_3}\right) + \frac{d_{31}}{h_1} v\right] \tag{4.12}$$

To facilitate analysis, the following expressions are used for nondimensionalization.

$$W = \frac{w}{L} \tag{4.13}$$

$$X = \frac{x}{L} \tag{4.14}$$

$$V = \frac{v d_{31}}{h_1} \tag{4.15}$$

$$G = \frac{g_2 L^2}{h_1 h_2}\left(\frac{1}{E_1} + \frac{h_1}{h_3 E_3}\right) \tag{4.16}$$

$$\sigma = \frac{\sigma_1 L b h_1 \beta}{E_3 I_3} \tag{4.17}$$

$$A = \frac{L b h_1 \beta E_1 E_3 h_3}{E_3 I_3 (h_3 E_3 + h_1 E_1)} \tag{4.18}$$

$$B = \frac{h_3}{2L} \tag{4.19}$$

$$T = t\sqrt{\frac{E_3 I_3}{\rho b h_3 L^4}} \tag{4.20}$$

$$\tau = \frac{\tau_2 L^2 b \beta}{E_3 I_3} \tag{4.21}$$

$$J = \frac{J_t}{\rho b h_3 L^3} \tag{4.22}$$

$$M = \frac{M_t}{\rho b h_3 L} \tag{4.23}$$

$$r = \frac{\beta}{L} \tag{4.24}$$

The final set of equations is then:

$$\frac{\partial^4 W}{\partial X^4} + \frac{\partial^2 W}{\partial T^2} = \frac{\partial^2 \sigma}{\partial X^2} \tag{4.25}$$

$$\frac{\partial^2 \sigma}{\partial X^2} - G\sigma = GAB\frac{\partial^2 W}{\partial X^2} + GAV \tag{4.26}$$

Combining Equations (4.14) and (4.15) yields the sixth order partial differential equation:

$$\frac{\partial^6 W}{\partial X^6} - G(1+AB)\frac{\partial^4 W}{\partial X^4} + \frac{\partial^4 W}{\partial X^2 \partial T^2} - G\frac{\partial^2 W}{\partial T^2} - AG\frac{\partial^2 V}{\partial X^2} = 0 \tag{4.27}$$

The governing differential equation is of sixth order, therefore six boundary conditions need to be specified. Four of these are the usual boundary conditions associated with beam end conditions. The beam boundary conditions which will be used here are those used in the earlier study, a cantilevered beam with tip mass and rotational inertia. They are given by Equations (4.28) to (4.31).

$$W = 0\Big|_{X=0} \tag{4.28}$$

$$\frac{\partial W}{\partial X} = 0\Big|_{X=0} \tag{4.29}$$

$$\frac{\partial^2 W}{\partial X^2} = -J\frac{\partial^3 W}{\partial T^2 \partial X} + V(t)\Big|_{X=1} \tag{4.30}$$

$$\frac{\partial^3 W}{\partial X^3} = M\frac{\partial^2 W}{\partial T^2}\Big|_{X=1} \tag{4.31}$$

The two additional boundary conditions are imposed on the VEM and constraining layer. A short listing of some candidate boundary conditions may be found in [26]. The boundary conditions chosen in this application are relatively simple. The first is specifying zero tensile stress in the constraining layer at the root end of the beam. This corresponds to a free end of the constraining layer. The second is specifying zero shear stress in the VEM at the tip. These boundary conditions are given by Equations (4.32) and (4.33) respectfully.

$$\frac{\partial^4 W}{\partial X^4} + \frac{\partial^2 W}{\partial t^2} - GAB\frac{\partial^2 W}{\partial X^2} - GAV = 0\Big|_{X=0} \tag{4.32}$$

$$\frac{\partial^6 W}{\partial X^5} + \frac{\partial^3 W}{\partial X \partial t^2} - GAB\frac{\partial^3 W}{\partial X^3} - GA\frac{\partial V}{\partial X} = 0\Big|_{X=1} \tag{4.33}$$

Figure 4.6 shows schematically a beam with these boundary conditions.

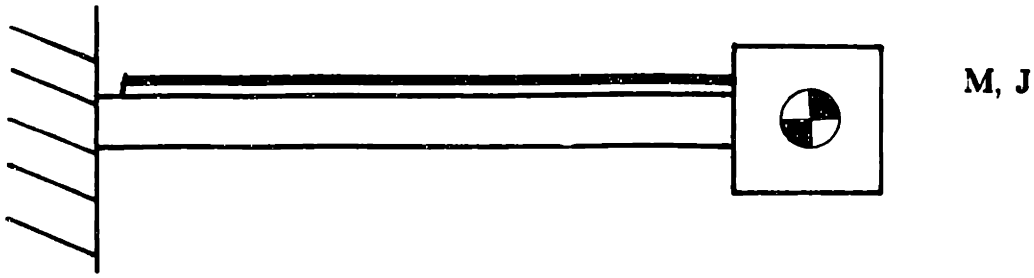

Figure 4.6: Cantilevered Beam with Active Constrained Layer Damper

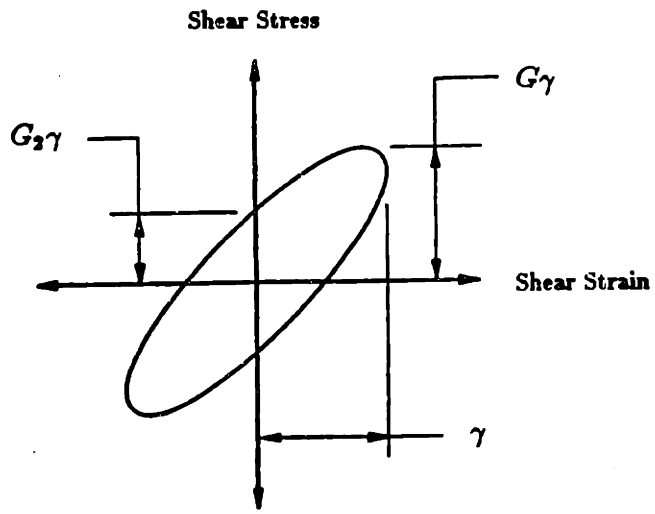

Figure 4.7: Hysteresis Loop of a Viscoelastic Material

4.3 Energy Dissipation with an Active Constrained Layer Damper

The energy removed from the structure will be due to two effects, dissipation within the shear layer, and active work done on the boundary. The internal dissipation can be further resolved into a passive component, which is present in all constrained layer dampers, and an active component which is due to the piezoelectrical properties of the constraining layer. These three distinct energy pathways, passive dissipation, active dissipation, and boundary work, will be discussed separately.

Energy dissipation within a viscoelastic material is a result of the stress and strain histories having components in quadrature with one another, and is equal to the area of the hysteresis loop of the material's stress-strain diagram. (cf. Figure 4.7) In the analysis that follows, forced, sinusoidal steady state vibrations are considered. This assumption allows the use of a complex shear modulus to

evaluate internal losses. The modulus is of the form

$$G = (G_1 + j \cdot G_2) \tag{4.34}$$

where G_1 and G_2 are the storage and loss moduli of the viscoelastic material. The ratio G_2/G_1 is commonly called the loss factor of the material. Appendix I gives a brief description on the use of a complex modulus in evaluating the strain response of a viscoelastic material to an applied stress.

The loss factor of a system with a passive constrained layer damper can be found using the approximate relationship [26]:

$$\eta = 12\phi\eta_2 \frac{\frac{E_1 h_1}{E_3 h_3}\left(\frac{\beta}{h_3}\right)^2}{1 + 2\phi + \phi^2(1 + \eta_2{}^2)} \tag{4.35}$$

$$\phi = \frac{g_2}{2\pi f E_1 h_1 h_2}\left(\frac{E_3 I_3}{\rho b h_3}\right)^{\frac{1}{2}} \tag{4.36}$$

Where ϕ is defined as the nondimensional shear parameter, and η_2 is the loss factor of the viscoelastic layer. The system loss factor is defined as the ratio of the energy dissipated per cycle to the peak strain energy in the structure during that cycle. For effective passive constrained layer designs, the shear parameter should be near unity [26]. For this reason passive constrained layer dampers can usually only be made effective for a single mode at a time.

A passive constrained layer damper which used PVF2 as the constraining layer was designed to damp the first mode of the 6 inch steel beam used in the Lyapunov damper tests. With this design, there were only two design variables which could be varied. They were the VEM shear modulus, and the VEM thickness. Given that there is a practical lower limit on the shear modulus of real materials, the design required a very thick shear layer to arrive at a low shear parameter. The passive design started with a very low modulus material found in the literature [27], and varied the thickness until the shear parameter equaled unity. The final design values appear in Table 4.1. The system loss factor for this design was $\eta = 0.098$. Although this is quite good, the design is a poor one. In order to achieve the desired shear parameter, the VEM thickness had to be increased until it was on the order of 8 beam thicknesses! Obviously this is an impractical design. The necessity of such a thick damping layer was a direct result of the low constraining layer stiffness. By comparison, using a steel constraining and the same VEM would yield a design with a similar loss factor, but a much thinner VEM layer. (cf. Table 4.2)

Alternatively, increasing the thickness of the PVF2 by a factor of three or four would produce reasonable designs.

The active effects of the damper are a result of piezoelectrically induced stresses. Since the system is linear, the stresses can be resolved into their active

Constraining Layer	PVF2
Thickness (m)	$2.5\text{x}10^{-5}$
VEM Modulus (Nm^{-2})	$1.58\text{x}10^{4}$
VEM Loss Factor	1.2
VEM Thickness (m)	$3.01\text{x}10^{-3}$
System Loss Factor	0.098
h_2/h_3	7.9

Table 4.1: Final Design Values of Passive Constrained Layer Damper Using PVF2 as the Constraining Layer

Constraining Layer	Steel
Thickness (m)	$2.5\text{x}10^{-5}$
VEM Modulus (Nm^{-2})	$1.58\text{x}10^{4}$
VEM Loss Factor	1.2
VEM Thickness (m)	$5.95\text{x}10^{-5}$
System Loss Factor	0.087
h_2/h_3	0.16

Table 4.2: Passive Constrained Layer Damper Design Using a Steel Constraining Layer

and passive components. The actively induced normal stress in the constraining layer can be found by setting the modal displacement of the beam to zero and solving equation (4.26), that is solving:

$$\frac{\partial^2 \sigma}{\partial X^2} - G\sigma = GAV \tag{4.37}$$

Using boundary conditions (4.32) and (4.33), this gives:

$$\sigma_V(X,T) = VA\left[\cosh(\sqrt{|G|}X) - 1 - \tanh(\sqrt{|G|}) \cdot \sinh(\sqrt{|G|}X)\right] \tag{4.38}$$

From equation (4.11), the active shear stress is found to be:

$$\tau_V(X,T) = VA\sqrt{|G|}\left[\sinh(\sqrt{|G|}X) - \tanh(\sqrt{|G|})\cosh(\sqrt{|G|}X)\right] \tag{4.39}$$

or more compactly:

$$\tau_V(X,T) = VA\sqrt{|G|} \cdot f(X) \tag{4.40}$$

The shear stress in the VEM which is due entirely to beam deflections will be denoted as $\tau_W(X,T)$. Thus the total shear stress in the VEM is given by Equation (4.41).

$$\tau(X,T) = \tau_V(X,T) + \tau_W(X,T) \tag{4.41}$$

The amount of energy actively dissipated per cycle of vibration will now be derived. It must be emphasized that although no control has been explicitly stated, the above analysis implicitly assumes that the shear stress is harmonic and in phase with the vibration. The work done on the viscoelastic layer is given by Equation (4.42).

$$\frac{du}{dV_{ol}} = \int_{t_1}^{t_2} \tau\dot{\gamma}dt \tag{4.42}$$

Assume harmonic motion with $\tau(t) = \tau_0\cos(\omega t)$ and a material with a complex shear compliance $C = C_1 + jC_2$. Then the work done on the material is given by Equation (4.43).

$$\frac{du}{dV_{ol}} = -\omega\int_{t_1}^{t_2} \tau_0^2 C_1 \cos(\omega t)\sin(\omega t)dt - \omega\int_{t_1}^{t_2} \tau_0^2 C_2 \cos^2(\omega t)dt \tag{4.43}$$

Let the limits of integration be one period of oscillation (i.e. 0 to $2\pi/\omega$) to find the energy storage and dissipation per cycle. The first term of Equation (4.43) is zero, and represents the elastic, recoverable work done during the cycle. The second term is given by:

$$\frac{du_{dis}}{dV_{ol}} = -\tau_0^2 C_2 \pi \tag{4.44}$$

This is the enery dissipated per cycle. Rewritten in terms of shear modulus parameters it becomes:

$$\frac{du_{dis}}{dV_{ol}} = \frac{r_0^2 g_2 \pi}{|g|^2} \tag{4.45}$$

The energy is nondimensionalized using Equation (4.46).

$$U = \frac{ul}{E_3 I_3} \tag{4.46}$$

The total energy dissipated is found by integrating over the volume of the shear layer. Substituting appropriate nondimensional parameters this becomes:

$$U = \frac{\pi G_2}{rA|G|^2} \int_0^1 r^2 dX \tag{4.47}$$

Making use of Equations (4.39) and (4.41) yields:

$$U = \frac{\pi G_2}{rA|G|^2} \int_0^1 \left[\tau_W + VA\sqrt{|G|} f(X)\right]^2 dX \tag{4.48}$$

Equation (4.48) shows that the amount of energy dissipated per cycle can be modulated actively.

In addition to internal dissipation, the active stresses appear in the boundary conditions. With the constraining layer fixed to the tip mass and left free at the root, the boundary conditions (4.30), (4.32) and (4.33) contain active terms. Equation (4.30) shows the normal stress in the constraining layer acts as a discrete moment at the beam tip. Since the tip may experience angular displacements, this moment can do work on the system. The active component of this boundary condition is just Equation (4.38) evaluated at $X = 1$.

$$\sigma(1,V) = VA\left(\frac{\cosh^2(\sqrt{|G|}) - \sinh^2(\sqrt{|G|})}{\cosh(\sqrt{|G|})} - 1\right) \tag{4.49}$$

Making use of the identity:

$$\cosh^2(u) - \sinh^2(u) = 1 \tag{4.50}$$

yields:

$$\sigma(1,V) = VA\left(\frac{1}{\cosh(\sqrt{|G|})} - 1\right) \tag{4.51}$$

The work done per cycle by this boundary condition is:

$$U(T) = V(T)A\left(\frac{1}{\cosh(\sqrt{|G|})} - 1\right) \cdot \frac{\partial W(1,T)}{\partial X} \tag{4.52}$$

This result is similar to those found by Bailey [9]. In the limit as the VEM stiffness tends toward infinity and the loss modulus goes to zero, Equation (4.52) and those derived in [9] are identical.

Boundary conditions (4.32) and (4.33) are both stress boundary conditions. Equation (4.32) requires the tensile stress in the constraining layer to be zero at the beam root. Equation (4.33) constrains the shear stress in the core to be zero at the tip. Since in each case the total stress is zero, there can be no resultant strain. Therefore neither boundary condition can do work on the system.

Chapter 5

Conclusions and Recommendations

5.1 Lyapunov Damper

An active vibration damper which uses a distributed piezoelectric actuator, and 'bang-bang' feedback control to damp transverse vibrations in beams has been tested experimentally on two different structures. One was a 6 inch x 0.5 inch x 0.030 inch steel cantilever beam with a 6.7 gram tip mass. The second was a 48 inch x 6 inch x 0.1250 inch aluminum cantilever beam with a 2.04 kg tip mass. The results of tests on the first bending mode of these structures verify those results predicted by the simulation algorithm developed in [9].

Free vibration tests of the first mode of the steel beam were conducted by displacing the tip 2 cm, and releasing it. A beam without active control had a settling time of over 2 minutes. Free decay tests using the Lyapunov control algorithm and a control amplitude of 500 volts decreased the settling time to 8 seconds. Similar first mode tests were performed on the aluminum beam. The initial conditions for these tests was a tip displacement of 16.7 cm. Without active control the beam vibrations had a decay time of over 400 seconds. Using Lyapunov control with a control amplitude of 400 volts reduced this settling time to 126 seconds.

The active Lyapunov damping demonstrated in this study is nonlinear. If it were applied to a structure which had no internal damping, the tip displacement would decay linearly in time. This indicates a changing system loss factor. Using moderate feedback voltages, the effective loss factor of the closed loop system increased dramatically as the vibration level decreased. The passive loss factor of the steel beam was $\eta = 0.002$ for small amplitude tip displacements. Using the Lyapunov damper with an amplitude of 100 volts increased the loss factor to $\eta_{100} = 0.046$ at a tip displacement of 0.5mm. Active damping with a 500 volt control amplitude increased the loss factor to $\eta_{500} = 0.375$ at the same

displacement amplitude.

The passive loss factor at small tip displacements of the aluminum beam was $\eta = 0.0019$. Lyapunov control with an amplitude of 100 volts increased the system loss factor to $\eta_{100} = 0.030$ at a tip displacement amplitude of 1.7 cm. Active damping with a control amplitude of 400 volts increased the loss factor to $\eta_{400} = 0.080$.

The Lyapunov damper was also demonstrated to be very effective on the second and third bending modes of the aluminum beam. The initial conditions for these tests were established by using the film actuator to excite the beam at the desired modal frequency. The Lyapunov control algorithm used on the first mode tests was also used for these tests unchanged. For the second mode of the aluminum beam, the initial condition was an angular acceleration at the tip of 56.5 $rad\ s^{-2}$. The Lyapunov control decreased the settling time from a free decay of 41 seconds to a controlled settling time of 7.4 seconds using a control amplitude of 400 volts. The initial condition for the third mode tests was an angular acceleration of 127 $rad\ s^{-2}$ at the tip. For the third mode the settling time was reduced from 20.5 seconds to 3.8 seconds using a control amplitude of 400 volts.

These experimental results verify that the Lyapunov damping is most effective for smaller vibration levels. This is because the nonlinear damping dissipates an increasing percentage of the system energy as the vibration amplitude decreases. This type of active damping may be most effective as a method of keeping resonant vibrations from building up due to the potentially high levels of damping that can be achieved for low level vibrations.

5.2 Active Constrained Layer Damper

A constrained layer damper which uses the PVF2 acutator as an active constraining layer was proposed as a candidate design which would be effective on damping all vibration amplitudes. The general system consisting of a base structure, viscoelastic layer and active constraining layer was modelled, resulting in a sixth order partial differential equation governing the transverse motions of the beam. The specific case of the active constrained layer damper applied to a cantilevered beam with tip mass and rotary inertia was discussed. This model revealed that there are two ways the active constraining layer affects the beam. The first is by contributing to the shear strain in the VEM. As a result it is possible to actively modulate the amount of energy dissipated.

In addition to the internal disipation, the active control appears as work at the system boundary. With the constraining layer fixed to the tip mass and left free at the root, the active portion of the stress in the constraining layer appears as a boundary moment which can do work on the system. This result is similar to those found by Bailey [9] and is the basis of the Lyapunov control algorithm. In

the limit as the VEM becomes perfectly rigid and the loss modulus goes to zero, the model of the active constrained layer damper and the Lyapunov controller are identical. If the VEM has finite storage and loss moduli, the system will be affected by both the active dissipation and the boundary work.

5.3 Recomendations for Future Work

Future work in active vibration damping using PVF2 should address the following concerns: An optimality condition and a feedback control law for the active constrained layer damper should be derived. This will allow the effectiveness of this damper to be evaluated quantitatively. As a first step, the mode shapes that satisfy Equation (4.27) will have to be found.

The evaluation of the Lyapunov controller could be aided greatly by better measurement techniques of appropriate system parameters. Especially critical is the measurement of the moment constant. Experimental values obtained in this study and previous work [9] have shown discrepancies between predicted and observed values. In the aluminum beam tests, the moment constant was difficult to secure due to the fact that the first mode frequency was near the thermal drift frequency of the measurement equipment. Developing another technique, perhaps a dynamic test, should be considered. The higher mode experiments have shown that the PVF2 film can be used as an actuator quite effectively. It may be possible to derive the moment constant by measuring the steady state amplitude of forced vibrations and the modal damping.

A final area of recomended research is in using the film as a distributed sensor. Crude experiments have shown that a large output voltage is generated by the film when the beams were excited harmonically. Transient tests have also shown that the film output spectrum and the beam modal spectrum were the same.

Appendix A

Viscoelastic Response to an Applied Stress

Using the Euler definition of the complex expontential (A.1),

$$e^{j\omega t} = \cos(\omega t) + j \cdot \sin(\omega t) \tag{A.1}$$

along with the complex shear modulus greatly simplifies the task of identifying the strains which are in phase and in quadrature with the stress. Consider a viscoelastic material being sheared by an applied stress given by Equation (A.2), which can also be written as the real part of the complex function (A.3).

$$\tau = \tau_0 \cdot \cos(\omega t) \tag{A.2}$$

$$\tau = Re\left(\tau_0 \cdot e^{j\omega t}\right) \tag{A.3}$$

Assume the material can be characterized by a complex shear compliance, C.

$$C = \frac{1}{G} \tag{A.4}$$

$$C = \frac{1}{G_1 + j \cdot G_2} \tag{A.5}$$

$$C = \frac{G_1}{G_1^2 + G_2^2} - j \cdot \frac{G_2}{G_1^2 + G_2^2} \tag{A.6}$$

Then, the shear strain is given by Equation (A.7).

$$\gamma = (C_1 + j \cdot C_2) \cdot \tau_0 \cdot e^{j\omega t} \tag{A.7}$$

Since the forcing function has been defined as the real portion of equation (A.3), it is appropriate to use only the real part of Equation (A.7) as the solution.

$$\gamma = \tau_0 \cdot (C_1 \cos(\omega t) - C_2 \sin(\omega t)) \tag{A.8}$$

Equation (A.8) consists of two terms, one in phase with the forcing function, and one in quadrature with it. Equation (A.8) can be rewritten in terms of elastic modulus by substituting Equation (A.6) into (A.8).

References

1. W.E. Vander Velde and C.R. Carigan, "Number and Placement of Control System Components Considering Possible Failures," MIT Space Systems Laboratory Report No. 5-82, March 1981

2. R.W. Trudell, R.C. Curley and L.C. Rogers, "Passive Damping in Large Precision Space Structures," AIAA 80-0667, 1980

3. L. Mierovitch (ed.), "Dynamics and Control of Large Flexible Spacecraft," Proceedings of a Symposium held in Blacksburg, VA, June 13-15, 1977.

4. L. Mierovitch (ed.), "Dynamics and Control of Large Flexible Spacecraft," Proceedings of the Second VPI/AIAA Symposium held in Blacksburg, VA, June 21-23, 1979.

5. L. Mierovitch (ed.), "Dynamics and Control of Large Flexible Spacecraft," Proceedings of the Third VPI/AIAA Symposium held in Blacksburg, VA, June 15-17, 1981.

6. M.G. Kelley, W. Podgorski, and J.E. Hubbard Jr., "Mechanical Design of a Flexible Spacecraft Test Modal for Active Vibration Control," AIAA preprint no. AIAA-84-1048-CP, presented at the 25th Structural dynamics Conference, Palm Springs, CA, 1984.

7. "Passive and Active Suppression of Vibration Response on Precision Structures, State-of-the-Art Assessment," Technical Analysis, Technical Report R-1138, Vol. 2, The Charles Stark Draper Laboratory, Inc., Cambridge Mass., 1978

8. S.E. Burke and J.E. Hubbard Jr., "Distributed Parameter Control Design For Vibrating Beams Using Generalized Functions," to be presented at the Fourth IFAC Symposium on Control of Distributed Parameter Systems, Pasadena, CA, June 30 - July 2, 1986.

9. T. Bailey, "Distributed Parameter Active Vibration Control of a Cantilevered Beam Using a Distributed Parameter Actuator," MS/BS Thesis, Massachusetts Institute of Technology, September 1984.

10. T.C. Henderson, J.R. and Canavin, "Damping Augmentations for Large Space Structures," Ninth AIAA/ASME Structures and Materials Conference, Paper No. 78-490, Bethesda, Md. April 1978.

11. J.S. Gibson, "An Analysis of Optimal Model Regulation: Convergence and Stability," Siam Journal of Control and Optimization, vol. 19, No. 5, pp. 686-707, September, 1981.

12. L. Meirovitch and H. Bauh, "Nonlinear Control of an Experimental Beam by IMSC," AIAA preprint no. 83-0855.

13. M.J. Balas, "Active Control of Flexible Systems," Journal of Optimization Theory and Applications, vol. 25, no. 3; pp. 415-436, 1978.

14. S.S. Gates, "Member Dampers for Vibration Suppression of Large Space Structures," MS thesis, Mass. Inst. of Tech., September 1979

15. M.J.Balas, "Finite-Dimensional Controllers for Linear Distributed Parameter Systems: Exponential Stability Using Residual Mode Filters," to be presented at the Fourth IFAC Symposium on Control of Distributed Parameter Systems, Pasadena, CA, June 30 - July 2, 1986.

16. R.E. Kalmann and J.E. Bartram, "Control System Analysis and Design via the 'Second' Method of Lyanpunov," ASME Journal of Basic Engineering, pp. 371-400, 1960.

17. P.K.C. Wang, "Stability Analysis of Elastic and Aerelastic Systems via Lyapunov's Direct Method," Journal of Franklin Institute, Vol. 281, No. 1 pp. 51-72, January 1966.

18. M. Slemrod, "Stability Analysis of Elastic and Aeroelastic Systems via Lyapunov's Direct Method," Journal of Mathematical Analysis and Applications, 46(2), May 1974, pp. 369-387.

19. "Kynar Piezo Film," Product information from the Pennwalt Corp.. King of Prussia, PA, 1983

20. T. Bailey and J.E. Hubbard Jr., "Distributed Piezoelectric Polymer Active Vibration Control of a Cantilever Beam," AIAA Journal of Guidance and Control, Sept. 1985.

21. S.H. Crandall, N.C. Dahl, and T.J. Lardner, An Introduction to the Mechanics of Solids, second edition, McGraw-Hill Book Company, New York, 1978, p. 531

22. D. Ross, E.E. Unger, and E.M. Kerwin Jr., "Damping of Plate Flexural Vibrations by Means of Viscoelastic Laminae," ASME, Structural Damping, PP. 49-87, 1959

23. E.M. Kerwin Jr., "Macromechanism of Damping in Composite Structures," ASTM, 1965

24. J.M. Plump and J.E. Hubbard Jr., "Modelling of an Active Constrained Layer Damper," to be presented at The 12th International Congress on Acoustics, July 30th 1986, Toronto, Canada.

25. D.J. Mead and S. Markus, "The Forced Vibration of a Three-Layer, Damped Sandwitch Beam with Arbitrary Boundary Conditions," Journal of Sound and Vibration 10, pp. 163-175

26. E.E Ungar, "Damping Tapes for Vibration Control," Product Engineering, January 1960, pp.57-62

27. Course Notes, "Vibration Damping Short Course," The University of Dayton, Dayton Ohio, June 20, 1983, p.4.4-11